Monthly Notices
of the
ROYAL ASTRONOMICAL SOCIETY

MNRAS **469,** 4649–4664 (2017)
Advance Access publication 2017 April 5

doi:10.1093/mnras/stx818

The quest for blue supergiants: binary merger models for the evolution of the progenitor of SN 1987A

Athira Menon[1]★ and Alexander Heger[1,2,3]★

[1]*Monash Centre for Astrophysics (MoCA) and School of Physics and Astronomy, Monash University, Clayton, VIC 3800, Australia*
[2]*School of Physics and Astronomy, University of Minnesota, Minneapolis, MN 55455, USA*
[3]*Centre for Nuclear Astrophysics, Shanghai Jiao Tong University, Shanghai 200240, China*

Accepted 2017 March 29. Received 2017 February 9; in original form 2016 November 6

ABSTRACT

We present the results of a systematic stellar evolution study of binary mergers for blue supergiant (BSG) progenitors of Type II supernovae. In particular, these are the first evolutionary models that can simultaneously reproduce nearly all observational aspects of the progenitor of SN 1987A, Sk –69 °202, such as its position in the Hertzsprung–Russell diagram, the enrichment of helium and nitrogen in the triple-ring nebula and its lifetime before its explosion. The merger model, based on the one proposed by Podsiadlowski, Joss and Hsu, and Podsiadlowski, Morris and Ivanova, consists of a main-sequence secondary star that dissolves completely in the common envelope of the primary red supergiant at the end of their merger. We empirically explore a large initial parameter space – primary masses (15, 16 and 17 $M_\odot$), secondary masses (2, 3,..., 8 $M_\odot$) and different depths up to which the secondary penetrates the He core of the primary during the merger. The evolution of the merged star is continued until just before iron-core collapse, and the surface properties of the 84 pre-supernova models (of 16–23 $M_\odot$) computed have been made available in this work. Within the parameter space studied, the majority of the models are compact, hot BSGs with effective temperature >12 kK and radii of 30–70 $R_\odot$, of which six match the observational constraints of Sk –69 °202.

Key words: binaries: general – supergiants.

1 INTRODUCTION

The remarkable supernova SN 1987A that exploded in the Large Magellanic Cloud (LMC; West et al. 1987) is unique in many regards. Although initially classified as a sub-luminous Type II Plateau supernova (Type II-P SN) due to the presence of H I lines in its optical spectrum, it had an unusual dome-shaped light curve. The light curve of SN 1987A began to rapidly rebrighten after its initial decline, by a factor of 100 in a few hours as against days for Type II-P SNe, and at its maximum was only ∼10 per cent as luminous as most Type II-P SNe (Arnett et al. 1989; McCray 1993). The dome-shaped light curve (Catchpole et al. 1988; Hamuy et al. 1988) indicated that the progenitor was not a typical red supergiant (RSG; $R \approx$ 500–1000 $R_\odot$) as was expected for all H-rich Type II SNe observed until then, but a compact blue supergiant (BSG). An examination of previous photographic plates of the explosion site confirmed that the progenitor was indeed a compact B3 Ia supergiant named Sk –69 °202 (Blanco et al. 1987; Walborn et al. 1987). From its absolute magnitude measurements and by calibrating it against other B3 supergiants in the LMC, the luminosity of Sk –69 °202 was deduced to be $\log(L/L_\odot) = 5.15$–5.45, with an effective temperature, $T_{\rm eff}$ = 15–18 kK (Woosley 1988; Woosley, Pinto & Weaver 1988; Arnett et al. 1989; Walborn et al. 1989). The radius of the star thus calculated was $R = (3 \pm 1) \times 10^{12}$ cm (≈28–58 $R_\odot$). Barkat & Wheeler (1989a) deduced a slightly less luminous and possibly cooler progenitor, with $\log L/L_\odot = 4.90$–5.11 and $T_{\rm eff} = 12$–19 kK.

Another unusual aspect of SN 1987A is the shape of the circumstellar material nebula ejected by the progenitor before its explosion. It is a complex, triple-ring nebular structure, distributed in an axisymmetric but extremely non-spherical manner (Wampler et al. 1990; Burrows et al. 1995; France et al. 2010). Fransson et al. (1989) and Lundqvist & Fransson (1996) measured He/H = 0.25 ± 0.05 (ratio by number of atoms), in the nebular material but more recent estimates have lowered this value to He/H = 0.17 ± 0.06 (Mattila et al. 2010) and 0.14 ± 0.06 (France et al. 2011). Nitrogen is also enhanced in the nebula relative to carbon and oxygen; Lundqvist & Fransson (1996) estimated number ratios of N/C ∼ 5 ± 2 and N/O ∼ 1.1 ± 0.4, while Mattila et al. (2010) reported N/O ∼ 1.5 ± 0.7. Older estimates for these ratios are N/C ∼ 8 ± 4 and 1.6 ± 0.8 (Arnett et al. 1989). These

★ E-mail: athira.menon@monash.edu (AM); alexander.heger@monash.edu (AH)

enhancements of helium and nitrogen in the circumstellar nebular material, indicate that the star underwent H-burning through the CNO cycle in some phase of its evolution (Saio, Nomoto & Kato 1988; Fransson et al. 1989; Sonneborn et al. 1997; France et al. 2011). Panagia et al. (1996) found that the outer rings are less enriched in N/C and N/O, by a factor of ∼3 than the corresponding values measured in the inner ring, thus concluding that the outer rings may have been ejected 10 kyr before the inner ring. These results were contested by Crotts & Heathcote (2000), who, through a kinematic study, deduced that all three rings were expelled ∼20 kyr before the supernova explosion. Maran et al. (2000) further supported this result through long-slit optical spectroscopic measurements of the CNO abundances of the rings and found no discrepancies between the inner and outer rings.

From the spectrum of the recombination phase, possible enhancements in *s*-process elements, Ba and Sr, were also detected (Mazzali, Lucy & Butler 1992; Mazzali & Chugai 1995). Another observational constraint for Sk –69 °202 came from the expansion velocity of the inner ring of the nebula, through which the dynamical age of the BSG was estimated as 15–20 kyr (Burrows et al. 1995; Smith et al. 1998; Crotts & Heathcote 2000). Most of the mass of the nebula resides in the inner ring; the outer rings each weighs $\sim 0.045\,M_\odot$ (Lundqvist & Fransson 1996). The total mass of the nebula is, however, uncertain, although estimates range between 0.34 (Crotts & Kunkel 1991) and $1.7\,M_\odot$ (Burrows et al. 1995; Sugerman et al. 2005a,b). It should be borne in mind, however, that these estimates are based on an hour glass model while the circumstellar nebula of SN 1987A is in the form of a triple-ring structure (Podsiadlowski, private communication).

Ring-shaped circumstellar nebulae have been found around other BSGs as well, such as MN18 (Gvaramadze et al. 2015), SBW1 (Smith et al. 2013; Smith, Groh and France 2017), HD 168625 (Smith 2007). An object that is considered a more luminous twin of Sk –69 °202 with luminosity $\log(L/L_\odot) = 5.78$–5.90 (Smartt et al. 2002; Melena et al. 2008) is Sher 25 located in the Milky Way. The nebula surrounding this BSG is enhanced in nitrogen (Smartt et al. 2002; Hendry et al. 2008) and has a similar hourglass morphology, mass and kinematics to the triple-ring nebula of SN 1987A (Brandner et al. 1997a,b). This is also the case for the central star and circumstellar ring structure of SBW1 (Smith et al. 2017), suggesting that these stars may have undergone a similar evolution as Sk –69 °202. Aside from BSGs with ring-shaped circumstellar nebulae, mergers may also be the origin of progenitors of superluminous Type II-P SNe (Vanbeveren et al. 2013; Justham et al. 2014) and of Type II-b SNe (Folatelli et al. 2015). Mergers may also have played a role in the formation of rapidly rotating B[e] supergiants (such as R4) and of supermassive objects such as η Carinae (Podsiadlowski et al. 2006).

Since the discovery of SN 1987A, 11 more supernovae have been recorded with similar dome-shaped light curves (Taddia et al. 2013), suggesting that they had BSG progenitors as well ($R \leq 70\,R_\odot$). These are collectively classified as Type II-peculiar supernovae (Type II-pec SNe) and have been mostly detected in low-metallicity environments (Pastorello et al. 2012; Taddia et al. 2013). These detections indicate they are rare events, forming only 1–3 per cent of known core-collapse SNe (Smartt 2009; Kleiser et al. 2011; Pastorello et al. 2012), while the majority are Type II-P SNe (Smartt 2009). This fraction of known Type II-pec SNe could change with more observations from blind and deeper surveys (zPTF, LSST; Dessart, private communication).

The evolutionary path that would form a BSG with the characteristics of Sk –69 °202, is not entirely certain. From single star evolutionary tracks, the initial mass of the progenitor was estimated to be $14-20\,M_\odot$ (ignoring mass loss, rotation and overshoot mixing) (Saio et al. 1988; Woosley 1988; Arnett et al. 1989). The typical evolution of stars in this mass range does not lead to BSG pre-supernova (pre-SN) models. Therefore, unusual evolutionary scenarios were invoked to explain how they could appear as BSGs before their explosion. These include models of low metallicity (Arnett et al. 1989), extreme mass-loss (Maeder 1987; Wood 1988), restricted-convection (Woosley et al. 1997; Langer 1991), helium-enrichment (Saio et al. 1988) and rapid-rotation (Weiss, Hillebrandt & Truran 1988; Hirschi, Meynet & Maeder 2004) (see Arnett et al. 1989; Podsiadlowski 1992; Smartt 2009 for a full review). The major difficulties in single-star models, however, are the extreme fine-tuning of parameters required to obtain the transition from red to blue in the Hertzsprung–Russell diagram (HRD) and their inability to reproduce the unusual composition of the circumstellar material. Most importantly, the single-star scenario cannot explain the complex geometry of the nebula and how it was ejected about 20 kyr before explosion. The single-star rotating model of Chita et al. (2008) does produce this nebular shape; however, the model does not end its life as a BSG.

Of particular insight and relevance to our study are the predictions of Barkat & Wheeler (1989b). In their parameterised study of single star models between 18–25 $M_\odot$, they showed that if the He core is penetrated by the H-rich envelope, the star would have a smaller He core to total mass ratio. This in turn could influence the star to turn from red to blue during its evolution. The core penetration would also lead to the dredge up of CNO-cycle processed material, thus enriching the surface of the star with He and N. Through a similar parameterised study applied to rotating single massive stars, Petermann et al. (2015) also demonstrated that models with smaller He cores than their inital values, could favour blue solutions. Barkat & Wheeler (1989b) mentioned another solution to obtain a small He core to total mass ratio–one where the primary star accretes mass from its companion in a binary system.

Chevalier & Soker (1989) were the first to predict the role of a binary system in the evolution of Sk –69 °202, by noting the asymmetrical expansion of the envelope of the supernova. Indeed, most massive stars are found in binary or multiple systems (Popova, Tutukov & Yungelson 1982), and of these, a substantial fraction (at least 20 per cent–60 per cent of stellar systems) are close enough to interact (Tutukov, Yungelson & Iben 1992; Kobulnicky & Fryer 2007; Eggleton & Tokovinin 2008; Sana et al. 2012, 2013).

Today, the most widely accepted binary scenario for Sk –69 °202 is that of a merger, the main evidence for which comes from the highly non-spherical shape of the triple-ring nebula (Podsiadlowski 1992; Morris & Podsiadlowski 2007; Podsiadlowski et al. 2007). Mergers of binary stars are expected to be the end result of ∼10 per cent of all massive stars, as indicated by population synthesis studies (Podsiadlowski, Joss & Hsu 1992; Podsiadlowski, Morris & Ivanova 2006). The first studies to investigate merger models for Sk –69 °202 are that of Hillebrandt & Meyer (1989), Podsiadlowski, Joss & Rappaport (1990) and Podsiadlowski et al. (1992). The scenario consists of a main-sequence secondary star merging with a primary RSG and dissolving completely in the envelope of the primary. A BSG model is formed either due to the enrichment of He in the envelope through dredge-up, which lowers the opacity of the surface (Hillebrandt & Meyer 1989), or due to the secondary being dumped on the primary, which increases the latter's envelope mass and thus decreases the core to total mass ratio (Podsiadlowski & Joss 1989; Podsiadlowski et al. 1990).

Our work is based on the merger model of Podsiadlowski et al. (1992), in which the evolution of the post-merger models were

tracked until carbon-ignition in the core; two of these models lay where Sk –69 °202 was observed in the HRD before its explosion (fig. 13 in Podsiadlowski et al. 1992). This merger scenario was further developed by performing hydrodynamic simulations of the merger (Ivanova et al. 2002; Ivanova 2002) and by studying the evolution of the models after the merger (Ivanova & Podsiadlowski 2002a,b). Morris & Podsiadlowski (2007, 2009) were also able to successfully construct the triple-ring nebula through hydrodynamic simulations of the mass ejected from the merger.

In its most recent version, the above merger scenario appears in Podsiadlowski et al. (2007). It begins with a wide binary system of a 15–20 $M_\odot$ primary and a 1–5 $M_\odot$ secondary, with an initial orbital period greater than 10 yr. When the primary evolves to an RSG with a He-depleted core, it transfers mass on a dynamically unstable time-scale on the secondary main-sequence star leading to a CE episode, during which the envelope is partially ejected. The secondary star is engulfed by the envelope of the primary and eventually undergoes a merger over ∼100 yr (Ivanova et al. 2002; Ivanova & Podsiadlowski 2003). After thermally adjusting to its structure, the merged star is expected to contract to a rapidly rotating BSG that sheds additional mass and finally explodes as a Type II-pec SN. The hot and fast wind of the BSG sweeps up the circumstellar material and shapes it to the triple-ring nebular structure we currently observe (Chevalier & Dwarkadas 1995; Morris & Podsiadlowski 2007, 2009; Podsiadlowski et al. 2007). In Section 1.1, we provide a more detailed picture of the binary system and its merger.

In this work, we independently construct our evolutionary model based on the above merger scenario. We study the evolution of 84 initial systems, through the merger phase and until just before the onset of iron-core collapse. Of these, six models successfully reproduce the three signatures of Sk –69 °202: its position as a BSG in the HRD, its lifetime as a BSG before explosion and the high N/C, N/O and He/H ratios in its surface. These are the first pre-SN models in refereed literature to have obtained all the major characteristics of Sk –69 °202.

In the next section, we provide a more detailed picture of the binary scenario used in this work.

1.1 Binary merger scenario

This section is a review of the works relevant for our study and presents the merger scenario from Podsiadlowski et al. (1992); Podsiadlowski (1992); Podsiadlowski et al. (2006, 2007), the results of the 3D simulations of the merger by Ivanova et al. (2002) and the post-merger evolution of the 3D models in 1D as described in Ivanova & Podsiadlowski (2002a,b, 2003). The binary system in these works initially consists of a primary star (M_1 = 15–20 $M_\odot$) and a secondary (M_2 = 1–5 $M_\odot$) companion star, both on the main sequence, orbiting with an initial period greater than 10 yr. As the primary approaches core helium depletion, it expands to an RSG that consists of an He core (consisting of a CO core + He shell) and a convective envelope. It then overflows its Roche lobe and an unstable case C mass transfer ensues from the primary to the secondary, initiating a CE episode that engulfs the secondary. The system now consists of the He core of the primary and the main-sequence secondary inside the convective envelope. Due to viscous drag forces, the secondary spirals in rapidly towards the core and a fraction of the energy released during the orbital decay is transferred to the outer layers of the CE, spinning it up. When the total orbital energy deposited in the envelope becomes comparable to the envelope binding energy, the envelope expands and ejects some of its mass. The aspherical outer rings of the nebula may have formed from the mass ejected during this CE phase.

The spiral-in phase ends when the secondary overflows its Roche lobe (at a separation of about 10 $R_\odot$) and starts a stable mass transfer to the core of the primary, driven by the friction with the envelope in a period of the order of ∼100 yr. H-rich material from the secondary forms a stream during the accretion and penetrates the He core, causing it to shrink in mass. As the secondary mass accretes on the He core, it also gets mixed in the convective envelope of the primary. A fraction of the H-rich secondary mass also penetrates the He core, while an equivalent fraction of the He core is dredged up. The region just below the boundary of the He core is hot enough for the CNO cycle to operate, and this burns the fresh fuel of hydrogen to helium and nitrogen. The He core mass that is dredged up to the surface is thus enriched in helium and nitrogen. Mass continues to be transferred from the secondary until it finally gets dynamically disrupted and dissolved in the envelope of the primary.

At the end of the merger, the structure of the star consists of a smaller He core, surrounded by an envelope of homogenous chemical abundances, that comprises the envelope of the RSG primary, mixed with the mass of the secondary star and the material dredged up from the core. Such a merger, occurring over a time-scale of ∼100 yr, is classified as a 'moderate' merger. The remnant will immediately appear as an RSG out of thermal equilibrium, then contracts continuously towards hotter temperatures and higher luminosities in the HRD. The star thus transitions from the red to the blue part of the HRD and appears as a BSG rotating at near-critical velocity, which sheds mass to form the inner ring of the nebula. It is expected that the post-merger star would live as a BSG for about 15–20 kyr until its explosion (Heger & Langer 1998; Podsiadlowski et al. 2006).

The best-fitting hydrodynamic model of Morris & Podsiadlowski (2007), constructed on the basis of the above merger scenario, can successfully reproduce the triple-ring structure of the nebula, with a chosen inner ring mass of ∼0.4 $M_\odot$ and and an outer ring mass obtained from the merger itself, of ∼0.02 $M_\odot$ each. The ring mass has not been rigourously constrained and could be higher than current estimates, depending on how much angular momentum is lost from the spiral-in of the secondary (Podsiadlowski, private communication).

1.2 Aims and structure of this work

We build an 'effective-merger' model in 1D using the stellar evolution code KEPLER and follow the progress of the post-merger star until the onset of core collapse. Our aims are as follows:

(i) Run simulations over a grid of initial parameter space consisting of primary and secondary masses and the boundary of mixing in the He core during the merger. These are the three major aspects that control the outcome of the merger.

(ii) Analyse the distribution of models in the HRD and the number ratios of nitrogen to carbon and oxygen (N/C and N/O) and helium to hydrogen (He/H) in the surface and determine how the choice of initial parameters affects the final models.

(iii) Identify progenitor candidates of SN 1987A that match the observed characteristics of Sk –69 °202.

We describe the code employed, the construction of our effective-merger model, the initial parameters and models in Section 2. We present the pre-SN models and how the choice of initial parameters affect them in Section 3. Finally, we discuss our results and enlist the conclusions of our study in Section 4.

2 METHODOLOGY

2.1 The stellar evolution code: KEPLER

Based on the binary merger scenario in Section 1.1, we use KEPLER, an implicit one-dimensional (1D) hydrodynamics code that can compute stellar evolution models with rotation and nucleosynthesis (Heger, Langer & Woosley 2000; Woosley, Heger & Weaver 2002; Heger, Woosley & Spruit 2005; Woosley & Heger 2007). The code uses the Ledoux criterion for convection. Energy generation follows a 19-isotope nuclear reaction network prior to oxygen depletion and a 128-isotope quasi-equilibrium network thereafter. A detailed description of the nuclear reaction rates used for energy generation can be found in Rauscher et al. (2002) and Heger et al. (2002). The physics of rotation in the stellar interior includes angular momentum transport, time-dependent mixing from various rotational instabilities, along with magnetic torques, turbulent viscosities and diffusivities from the dynamo model (please refer to Heger et al. 2000, Heger & Langer 2000 and Heger et al. 2005 for more details). Mass-loss in the models arise from rotationally modulated winds (Heger et al. 2000) and mass-loss prescriptions, as described in Nieuwenhuijzen & de Jager (1990). The pre-SN model is generated by the code when the evolution terminates at the onset of core-collapse, which occurs when the infall velocity is 9×10^7 cm s^{-1}. Due to convergence problems during the simulations, some of the models crash in the last few time-steps during core-silicon burning, before reaching the pre-SN stage. We cannot hence provide an estimate of their iron core mass ($M_{\mathrm{Fe\,c}}$). The surface quantities of these models however, do not change over such small time-steps of the order of hours. Therefore the radius, effective temperature, luminosity and chemical abundances of these models will be the same as those expected from their pre-SN models.

We recently updated the opacity tables in KEPLER that previously consisted only of Type I OPAL tables (Iglesias & Rogers 1996; Weiss, private communication) to include α-enhanced Type I OPAL tables, Type II CO-enhanced OPAL tables, conductive opacities (Potekhin et al. 2006) and molecular opacities (Ferguson 2005). The opacities (Table 1) and the routines for interpolating them in metallicity, temperature, density, hydrogen mass fractions and enhancements in C, N, O and Ne were obtained from Boothroyd's homepage (http://www.cita.utoronto.ca/~boothroy/kappa.html). Routines to vary opacity from changes in CNO abundances due to nuclear burning were also included. For temperatures lower than 10^4 K, composition-dependent low-temperature Rosseland mean opacities were computed with AESOPUS (Marigo & Aringer 2009), which includes various sources of atomic, molecular and collision-induced opacities. The routine to interpolate these opacities was provided by Dr Thomas Constantino (Constantino et al. 2014).

The new opacities are smaller compared to the values obtained from the old tables. The overall effective temperature and luminosity of the pre-SN models increase significantly with these smaller opacities. The role of correct opacities is thus crucial in determining the evolutionary path of the star.

Table 1. Opacity tables with temperature and density regimes. $\log R = \log \rho - 3\,(\log T - 6)$, where ρ and T are in cgs units.

Opacity tables	$\log \rho$ (g cm^{-3})	$\log T$ (K)
OPAL 1995	−8.0 to 1.0	3.75–8.70
Conductive opacities	0.0–7.0	3–9
Low-temperature opacities	−8.0 to 1.0	≤4

2.2 Effective-merger model

Our 1D effective-merger model is based on the processes outlined in Section 1.1. The merging phenomenon is characterized by the simultaneous accretion and mixing of the secondary star in the envelope of the primary.

In this model, we assume merging follows immediately after the primary of main-sequence mass M_1 evolves to become the required pre-merger RSG model (as will be described in Section 2.3) whose mass is M_{RSG} and consists of an He core of mass $M_{\mathrm{He\,c,\,1}}$. M_{RSG} is slightly smaller than M_1 by $\approx$0.01 M$_\odot$ due to mass-loss through winds. From the hydrodynamic simulations described in Section 1.1, the merging phase is of the order of 100 yr, and so in our scenario, we choose a fixed merging period of 100 yr. This merging time-scale is much shorter than the thermal time-scale of the envelope, some 1000 yr, yet the thermal time-scale is short compared to the lifetime of the post-merger star before its explosion (of the order of 10^4 –10^5 yr); hence, varying the merging period within an order of 100 yr does not affect the post-merger evolution in any significant way. The rate of accretion is $M_2/100$ yr, and for the range of M_2 we choose, this leads to accretion rates of $\dot{M}_{\mathrm{acc}} = 0.02-0.08\,\mathrm{M}_\odot\,\mathrm{yr}^{-1}$. M_2 is accreted with the same entropy and angular momentum as that of the surface of the primary.

From the merger scenario, we know that the secondary star is entirely disrupted and mixed in the convective envelope of the primary by the end of the merger (Ivanova & Podsiadlowski 2002a,b, 2003). We implement this merging in our models by accreting a secondary star of uniform chemical composition on the primary RSG. In order to obtain this composition, the secondary main-sequence star is evolved to the same age as that of the RSG, and then the total masses of individual isotopes are averaged over M_2.

As M_2 gets accreted on the primary, it is also simultaneously mixed throughout its envelope. This mixing phenomenon is implemented through a Lagrangian mixing recipe, wherein each unit of M_2 accreted per time-step of the code ($\dot{M}_{\mathrm{acc}} \times \mathrm{d}t$) is mixed down progressively in mass to a boundary we specify, m_{b}, inside $M_{\mathrm{He\,c,\,1}}$. The He core (or the H-free core) mass is defined as the mass within which the hydrogen mass fraction drops to below $\sim 10^{-2}$. As a fraction of M_2 penetrates the He core of the primary, it brings down H-rich material and thus shrinks the mass of the He core, while an equivalent fraction (f_{c}) of $M_{\mathrm{He\,c,\,1}}$ is dredged up and mixed uniformly in the envelope. The boundary of penetration or mixing, m_{b}, of the secondary is thus set by f_{c}; $m_{\mathrm{b}} = M_{\mathrm{He\,c,\,1}} - f_{\mathrm{c}} \times M_{\mathrm{He\,c,\,1}}$. Effectively, m_{b} determines the boundary of the He core of the merged star. Since, however, a convection zone forms during the merger at m_{b}, an additional amount of H-rich material is mixed down from the envelope, resulting in an He core boundary that is smaller by 7 per cent–22 per cent of m_{b}.

In this manner, by the end of the merger, we have a star that consists of a He core whose mass is smaller by a fraction f_{c}, and a massive homogenous envelope mixed with M_2 and $f_{\mathrm{c}} \times M_{\mathrm{He\,c,\,1}}$ (Fig. 1). The total mass of the post-merger star is $\approx M_{\mathrm{RSG}} + M_2$.

In this first study, the effective-merger we implement is a simplified model. We do not include any heating of the mass dumped by accretion nor do we track its angular momentum. We also do not compute the angular momentum loss post the CE phase, and, consequently, there is no additional momentum in the envelope or associated mass-loss in our models. Our BSG models do not reach break-up velocities after the RSG contracts; hence, no mass is shed from the system (aside from the <0.1M$_\odot$ through RSG winds) and we cannot provide predictions for the BSG wind. These processes require detailed hydrodynamic simulations and have been investigated in other works mentioned in Section 1.1.

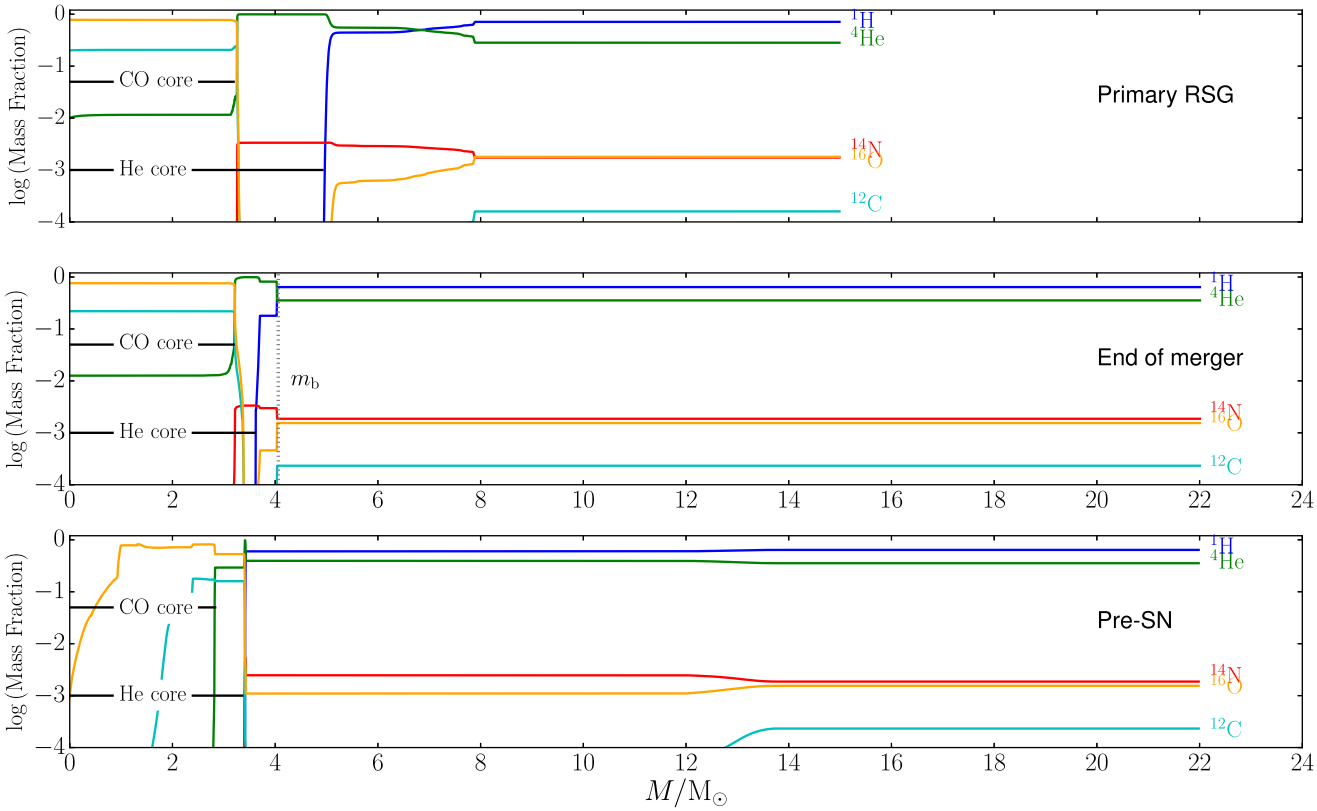

Figure 1. Top panel, stage B in Fig. 4: Composition of the RSG model from a primary of $M_1 = 16\,M_\odot$ consisting of a He core of $M_{\mathrm{He\,c,\,1}} = 4.92\,M_\odot$ just prior to the merger. Middle panel, stage C in Fig. 4: Composition at the end of the merger with $M_2 = 7\,M_\odot$. The boundary of mixing m_b (dotted vertical line) is set for $f_c = 16.6\%$. At the end of the merger, the star has a smaller He core of mass $3.41\,M_\odot$. Bottom panel, stage D in Fig. 4: Composition of the pre-SN model. The surface composition of the star does not change much from the one at the end of the merger.

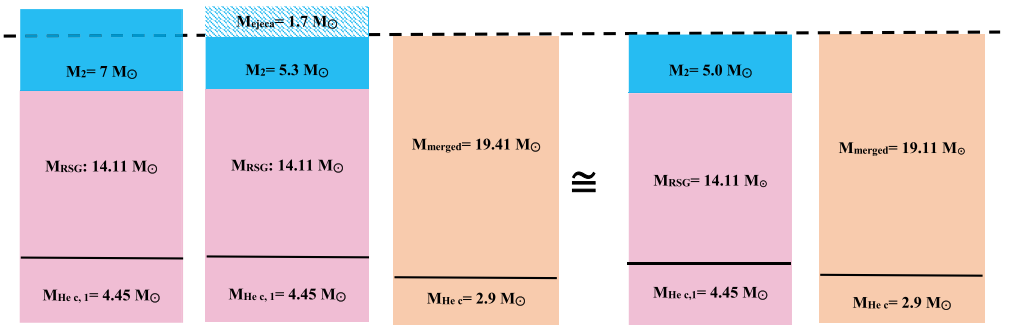

Figure 2. Diagram (not according to scale) showing the equivalence of mass ejection from the CE phase to accreting lower secondary masses.

Mass-loss is, however, an important effect, and it does play a significant role in the evolution of a star. Unfortunately, there does not exist an analytical prescription to calculate the mass ejected after the merger (Morris & Podsiadlowski 2009; Vanbeveren et al. 2013). The mass of the circumstellar nebula, currently estimated as $1.7\,M_\odot$, formed from the mass ejected in two stages – during the CE phase and when the post-merger RSG contracted to the BSG. Thus, the resultant mass of the star would be smaller by $1.7\,M_\odot$ than the sum of its components $M_{\mathrm{RSG}} + M_2$.

We account for the mass-ejection phenomenon indirectly – by accreting different values of M_2 on a particular RSG model. For example, let us take the merger of a system of $M_1 = 15\,M_\odot$ ($M_{\mathrm{RSG}} = 14.11\,M_\odot$) and $M_2 = 7\,M_\odot$, which will result in a star of $21.11\,M_\odot$. If $1.7\,M_\odot$ is ejected from the merger, this would reduce the total mass to $\approx 19.41\,M_\odot$. Equivalently, we can merge a system of $M_1 = 15\,M_\odot$ ($M_{\mathrm{RSG}} = 14.11\,M_\odot$) and $M_2 = 5\,M_\odot$, which would result in a star of $19.11\,M_\odot$, close to the mass obtained from the previous system (Fig. 2). The two systems will also have the same surface composition in the post-merger star. Thus, the post-merger evolutionary tracks obtained from both scenarios, the one with mass ejection and the one with a lower M_2, will be the same.

Fig. 3 outlines the evolutionary sequence for every system – we begin with the evolution of the primary star from the main sequence, merge it with a secondary mass and follow the evolution until the post-merger star attains an iron core just prior to core collapse. In the next section, we quantify the initial parameters chosen for our study.

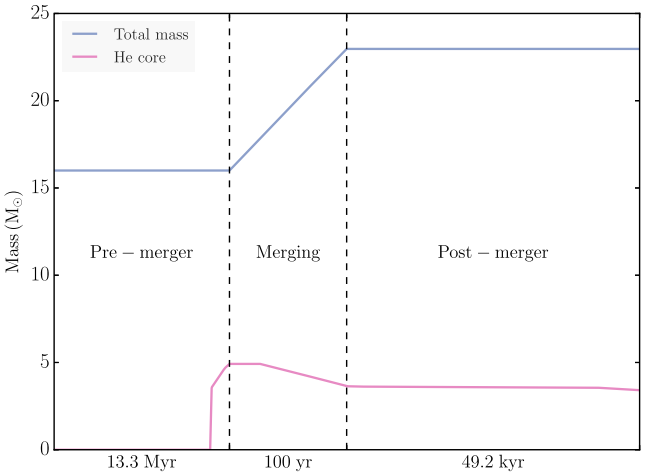

Figure 3. A schematic of the evolutionary sequence used in this work, illustrated for the system in Fig. 1. The primary is evolved until it becomes an RSG, over a period of 13.3 Myr, after which it is merged with the secondary over 100 yr. The post-merger model in this case is a BSG and it remains so for 49.2 kyr until its explosion. The He core mass is flat until ∼25 yr from the start of the merger before it begins to shrink. This is because it takes ∼25 yr for the boundary of the He core to recede due to dredge-up of H-rich material from the envelope.

2.3 Initial parameters

The primary and secondary stars are evolved from the main sequence with a solar-scaled composition of the LMC: $X_{\rm H} = 0.739$, $X_{\rm He} = 0.255$ and $Z = 0.0055$, which is 0.4 dex of the Asplund et al. (2009) solar metallicity, $Z_{\odot} = 0.014$. This metallicity is the value used by Brott et al. (2011), measured from observations of young massive stars in the H II regions of the LMC, although they use initial C, N, O values that are enhanced over solar in their work. As we shall discuss later, the metallicity is not the primary reason for stars becoming blue from mergers.

Our choice of main-sequence masses for the binary components is motivated by the mass predicted by single-star models for Sk –69 °202 and the merger scenario outlined by Podsiadlowski et al. (2007), i.e. $M_1 + M_2 = 18$–$22\,{\rm M}_{\odot}$. The primary RSG model chosen for the merger consists of a convective envelope and an He core with a central helium mass fraction of $X_{\rm He\,c,\,1} \sim 10^{-2}$ (Fig. 1). The primary main-sequence star has an initial rotational velocity at the equator of $\omega/\omega_{\rm crit} = 0.30$ ($v_{\rm eq} \approx 216\,{\rm km\,s^{-1}}$). When it becomes an RSG with a He-depleted core, its surface is enriched with the ashes of CNO-burning dredged up from the core to the envelope due to rotational mixing. Thus, the surface of the primary RSG model has high N/C and N/O ratios. Properties of the primary models used in this work are listed in Table 2.

The main-sequence masses of the secondary considered in this study are in the range $M_2 = 2$–$8\,{\rm M}_{\odot}$. Within the age of the primary RSG models (12.3–14.3 Myr, Table 2), the average isotopic abundances of the secondary masses vary only by a few per cent; $X_{\rm H}$ ($X_{\rm He}$) decreases (increases) by 8 per cent between $M_2 = 5$ and $10\,{\rm M}_{\odot}$. This does not significantly impact the evolution of the post-merger star or its abundances. Hence, we choose a 'standard' uniform isotopic composition for the accretion of secondary masses – that of a $5\,{\rm M}_{\odot}$ main-sequence star evolved until 14.3 Myr (Table 3).

Table 3. Uniform isotopic composition for the accreted secondary model. Isotope is the isotopic species; $X_{\rm f}$ is the mass fraction of accreted isotopes; $X_{\rm f}/X_{\rm i}$ is the change with respect to their initial values.

Isotope	$X_{\rm f}$	$X_{\rm f}/X_{\rm i}$
^{1}H	7.22×10^{-1}	0.98
^{4}He	2.72×10^{-1}	1.08
^{12}C	4.91×10^{-4}	0.50
^{14}N	1.28×10^{-4}	4.48
^{16}O	1.87×10^{-3}	0.80

The initial parameters that we vary are:

(i) Primary star mass (M_1): Models of the primary on the main sequence of mass $M_1 = 15, 16, 17\,{\rm M}_{\odot}$, and initial rotational velocity of $\omega/\omega_{\rm crit} = 0.30$ are evolved to the required RSG model (see the text above) for the merger.

(ii) Secondary star mass (M_2): Main-sequence star of a mass in the range $M_2 = 2$–$8\,{\rm M}_{\odot}$ is merged with each primary RSG model. The initial mass ratio (M_2/M_1) thus spans a range 0.12–0.53.

(iii) Fraction of He core of the primary dredged up ($f_{\rm c}$): For each combination of M_1 and M_2, we set the boundary of mixing $m_{\rm b}$ for M_2 by specifying $f_{\rm c}$, leading to $m_{\rm b} = M_{\rm He\,c,\,1} - f_{\rm c} \times M_{\rm He\,c,\,1}$. Increasing $f_{\rm c}$ results in larger fractions of the He core dredged up to the surface and smaller He cores for the post-merger star. It becomes instructive to use $f_{\rm sh}$, the fraction of He-shell mass of the He core dredged up, in place of $f_{\rm c}$, as we shall see in Section 3.

Thus, for every model, we choose a value of M_1 and M_2 and then choose a value for $f_{\rm c}$, which determines $m_{\rm b}$. By varying these three parameters, we establish a grid of 84 initial systems to study. In the next section, we explain the results of their evolution.

3 RESULTS

3.1 Progenitor models of SN 1987A

A successful SN 1987A progenitor model is one that satisfies the following criteria:

(i) The location of Sk –69 °202 in the HRD: $\log(L/{\rm L}_{\odot}) = 5.15$–$5.45$, $T_{\rm eff} = 15$–$18\,{\rm kK}$ and $R/{\rm R}_{\odot} = 28$–58 (Woosley 1988).

(ii) Surface number ratios match those of the circumstellar nebula; N/C $\sim 5 \pm 2$, N/O $\sim 1.1 \pm 0.4$ (Lundqvist & Fransson 1996) and He/H $= 0.14 \pm 0.06$ (France et al. 2011).

(iii) Lifetime of the post-merger BSG phase before explosion is at least 15 kyr.

Table 2. Parameters of the primary RSG models selected for merging. M_1 is the main-sequence mass of primary, $\omega/\omega_{\rm crit}$ is the initial rotational velocity on the main sequence; Age is the age of RSG model; $\tau_{\rm cc}$ is the time until core collapse; $M_{\rm RSG}$ is the mass of RSG model; $M_{\rm CO\,c,\,1}$ and $M_{\rm He\,c,\,1}$ are the masses of the CO core and the He core; $M_{\rm env,\,1}$ is the mass of the envelope, i.e. $M_{\rm RSG} - M_{\rm He\,c,\,1}$; and N/C, N/O and He/H are surface number ratios.

M_1 ($M_{\odot}$)	$\omega/\omega_{\rm crit}$	Age (Myr)	$\tau_{\rm cc}$ (kyr)	$M_{\rm RSG}$ ($M_{\odot}$)	$M_{\rm CO\,c,\,1}$ ($M_{\odot}$)	$M_{\rm He\,c,\,1}$ ($M_{\odot}$)	$M_{\rm env,\,1}$ ($M_{\odot}$)	N/C	N/O	He/H
15	0.30	14.35	20.2	14.11	2.89	4.45	9.66	10.1	1.09	0.10
16	0.30	13.28	21.2	15.04	3.25	4.87	10.17	9.2	1.12	0.10
17	0.30	12.33	37.8	15.87	3.62	5.26	10.61	9.5	0.75	0.10

Table 4. Parameters of the pre-SN models for SN 1987A. M_1 and M_2 are the initial primary and secondary masses of the binary system; f_{sh} and f_c are per cent fractions of He-shell mass and helium core mass that were dredged up; m_b is the boundary of mixing; $M_{He\,c}$, $M_{Fe\,c}$, M_{env} and $M_{pre\text{-}SN}$ are He core, iron core, envelope masses and mass of the pre-SN model ($M_c + M_{env}$); N/C, N/O and He/H are number ratios of nitrogen to carbon, nitrogen to oxygen and helium to hydrogen; T_{eff}, log (L) and $R_{pre\text{-}SN}$ are the effective temperature, luminosity and radius of pre-SN model; and τ_{BSG} is the lifetime of the BSG before explosion. '–' under the column $M_{Fe\,c}$ are for those runs that crashed while at core-silicon burning (refer to text in Section 2.1).

M_1 ($M_\odot$)	M_2 ($M_\odot$)	f_{sh} (per cent)	f_c (per cent)	m_b ($M_\odot$)	$M_{He\,c}$ ($M_\odot$)	M_{env} ($M_\odot$)	$M_{pre\text{-}SN}$ ($M_\odot$)	T_{eff} (kK)	log (L) ($L_\odot$)	$R_{pre\text{-}SN}$ ($R_\odot$)	$M_{Fe\,c}$ ($M_\odot$)	N/C	N/O	He/H	τ_{BSG} (kyr)
15	7	50	17.5	3.67	2.90	18.16	21.06	16.0	4.89	36.7	1.46	6.5	1.3	0.13	82
15	8	50	17.5	3.67	2.95	19.10	22.05	17.8	4.95	31.8	1.39	5.8	1.3	0.13	83
16	4	10	3.30	4.71	4.11	14.89	19.00	16.8	4.95	35.3	1.65	6.6	1.4	0.13	41
16	7	50	16.6	4.06	3.41	18.57	21.98	17.1	5.02	36.8	–	6.9	1.4	0.14	49
17	7	10	15.6	4.44	3.86	18.95	22.81	16.2	5.02	34.5	1.65	7.0	1.4	0.14	41
17	8	10	15.6	4.44	3.83	19.98	23.81	17.1	5.06	33.4	–	6.4	1.4	0.14	41

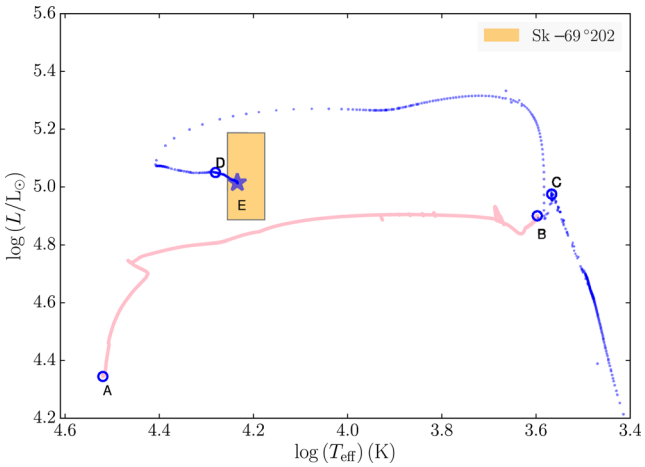

Figure 4. Evolutionary track of the merger of $M_1 = 16$ and $M_2 = 7\,M_\odot$, with $f_c = 16.6$ per cent. The shaded orange region represents observational limits for Sk –69 °202 by Woosley (1988) for T_{eff} and log ($L/L_\odot$). A and B: from the zero-age main sequence of the primary to the required RSG model. B and C: merger with the secondary. C and D: evolution of the post-merger model until carbon ignition in the core. D and E: further evolution to the final model just before core collapse. The final model (E) satisfies conditions (i)–(iii) in Section 3.1.

We classify our pre-SN models as Blue supergiants (BSGs), Yellow supergiants (YSGs) and Red supergiants (RSGs), based on their T_{eff} as follows:

(i) BSG: $T_{eff} \geq 12$ kK;
(ii) YSG: 12 kK $< T_{eff} \leq 4$ kK;
(iii) RSG: $T_{eff} < 4$ kK.

The evolution of one of the models that resembles the progenitor of SN 1987A ($M_1 = 16\,M_\odot$, $M_2 = 7\,M_\odot$ and $f_c = 16.6$ per cent, see Table 4) is shown in the HRD in Fig. 4 and in the schematic Fig. 3. Beginning from the zero-age main sequence (ZAMS) model (A), the primary inflates to an RSG with a He-depleted core over a period of 13.3 Myr (B). At this stage, the time until core collapse is 21.1 kyr. The merger is initiated immediately at point B and the secondary is accreted and mixed with the envelope of the primary until point C over 100 yr. During the merging process, the star goes out of thermal equilibrium and the code takes small time-steps to evolve it, resulting in a noisy phase on the HRD (the extended dotted blue line in Fig. 4). Due to the penetration of H-rich material, the He core mass shrinks, thereby increasing the lifespan of the post-merger star (by nearly 28 kyr) before it explodes. The H-fuel deposited increases the mass of the H-burning shell and its resulting higher luminosity pushes the convective envelope outwards, causing the star to inflate after the merger. When the convective envelope stops expanding and begins to recede, the star contracts and evolves towards the blue part of the HRD. At a certain point in its evolution, the convective envelope stops receding and begins to expand again causing the star to loop back to the red. It then undergoes carbon ignition in the core (D) and subsequent stages of nuclear burning and the evolution is stopped until just before the onset of iron-core collapse (E). The lifespan of this BSG model is 49.2 kyr before core collapse.

3.2 What factors affect the formation of BSGs?

Of the 84 models computed, 59 are BSGs and 25 are YSGs. Six of the BSGs qualify as progenitor models of SN 1987A, in accordance with the criteria (i)–(iii) in Section 3.1 (Figs 7 and 11) and are summarized in Table 4. We find that RSG pre-SN models result from mergers only if dredge-up occurs from the envelope, i.e. the He core is not penetrated, as will be discussed in the following sections.

We shall now investigate how the criteria in (i)–(iii) are affected by the input parameters of our model.

3.2.1 Surface N/C and N/O ratios

The envelope of the RSG primary model at the time of merger is already enhanced in nitrogen at the surface due to rotational mixing, as explained in Section 2.3 (also see Fig. 1, top panel). Depending on the values of M_2 and f_c, the N/C and N/O in the envelope will change as explained below.

Our choice for the mixing boundary m_b being set inside the He core is motivated by two factors – first, we know from hydrodynamic simulations that the He core is penetrated by a fraction of the secondary mass during the merger, and second, from our simulations, we find that the surface ratios of N/C and N/O are sensitive to the position of m_b. In Fig. 5, we demonstrate this for the case of $M_1 = 15$ and $M_2 = 5\,M_\odot$ with varying amounts of f_c. The larger f_c is, the deeper m_b is set inside the He core, resulting in larger amounts of $M_{He\,c,\,1}$ being mixed in the envelope during the merger. This is because the He shell, between the boundary of the CO core and He core, is nitrogen-rich (Fig. 1). Thus, in order to obtain high N/C and N/O ratios at the surface of the merged star, the boundary of dredge-up during the merger must be set within the He-shell region. If this boundary is set within the CO core, the mass dredged up from within the CO core to the surface will be rich in carbon and oxygen, thereby reducing N/C and N/O. Since we restrict mixing

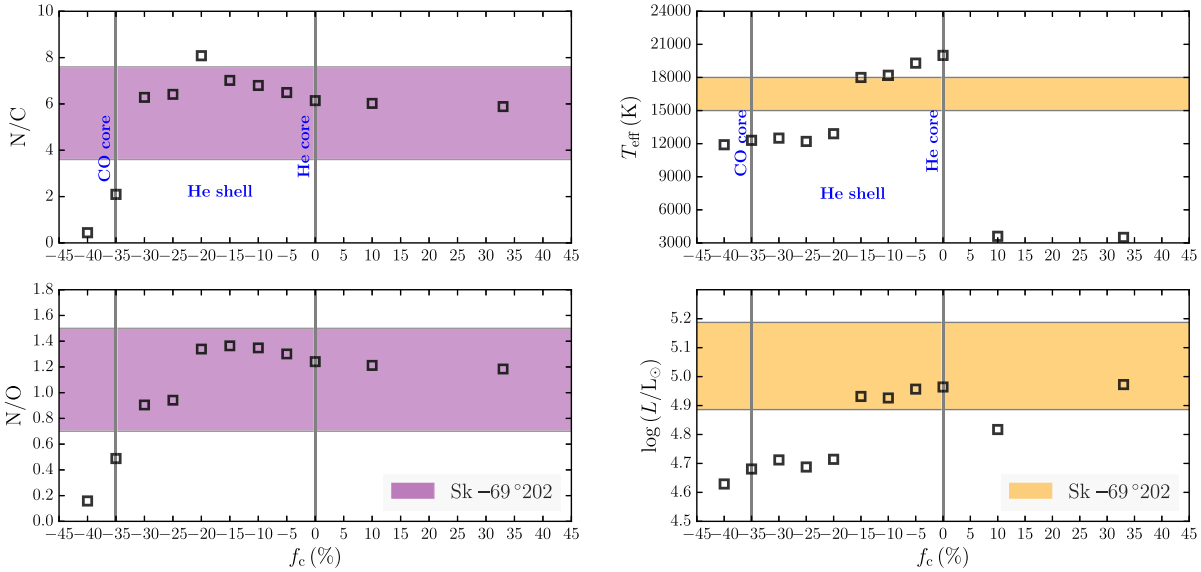

Figure 5. Surface quantities of pre-SN models obtained from the merger of $M_1 = 15$ and $M_2 = 5\,M_\odot$ with various dredge-up fractions of the He core (f_c in per cent). Left-hand panel: number ratios, N/C and N/O. Right-hand panel: effective temperature (T_{eff}) and luminosity (L). Negative values of f_c represent the case for which the He core of the primary is penetrated and positive values show the case for which the mixing is restricted to above the He core of the primary. Also marked are the boundaries of the CO core, He core and the He shell of the primary. The shaded regions denote observation limits for Sk –69 °202; the violet region limits are taken from Lundqvist & Fransson (1996) and the orange region limits are taken from from Woosley (1988).

to be inside the He shell, we use f_{sh}, the fraction of He-shell mass dredged up, to set m_b.

Two models are also computed for the case for which m_b is set outside the He core of the primary, i.e. the envelope does not penetrate the He core. For this case, since mass is dredged up from within the homogeneous envelope, the surface values of N/C and N/O are unchanged from their initial amounts.

We now demonstrate how these quantities vary for all the binary systems studied in this work, spanning the entire initial parameter space of M_1, M_2 and $f_{sh} = 10$ per cent, 50 per cent, 90 per cent and 100 per cent (Fig. 6). A table containing details of all the pre-SN models computed in this work is provided in Appendix A. As M_2 increases for a fixed f_{sh}, N/C and N/O decrease again. This is because the envelope mass increases as M_2 increases, causing the amount of nitrogen dredged up to be diluted in the envelope, thereby decreasing its mass fraction at the surface. As M_1 increases, the RSG models are increasingly enhanced in N/C and N/O at the surface (Table 2). Therefore for a given M_2 and f_{sh}, the values of N/C and N/O at the surface after the merger also increase in proportion to M_1.

From Fig. 7, the BSG pre-SN models from our simulations span a large range in surface ratios of N/C and N/O (Fig. 7), indicating that there is no correlation between being a BSG and having high values of N/C and N/O at the surface, i.e. these parameters are independent of each other. The YSG models (except for two) are somewhat more constrained, since they are less enriched in N/C and N/O at the surface than BSGs (N/O < 1.0, N/C < 9.7). The ratio He/H at the surface does not vary significantly for the parameter range we use, and is between 0.13 and 0.17 for all the pre-SN models.

3.2.2 *Effective temperature, luminosity and radius*

Varying f_c affects the effective temperature, T_{eff}, and luminosity, L, of the merged star (Fig. 5). For a fixed primary and secondary mass, increasing f_c (or f_{sh}) decreases the He core mass and causes T_{eff} and L to also decrease. In particular, for these models, dredging up more than 15 per cent of $M_{He\,c,\,1}$ (50 per cent of the He-shell mass), brings down T_{eff} from 18 to nearly 12 kK, and it remains more or less constant for larger values of f_c.

It is interesting to note that the case where m_b is set on the boundary of the CO core (i.e. $f_c = 0$) also becomes a BSG ($T_{eff} \approx 20$ kK). In the two models where m_b is set above the He core, the post-merger star explodes as a cool RSG of $T_{eff} = 3$ kK.

By increasing f_{sh} (Fig. 8), the secondary star mixes deeper inside the He core and the stars become brighter and hotter after the merger but evolve further from the bluest point of their evolution to the cooler and less luminous regions of the HRD. Thus, reducing the He core mass for a given M_1 and M_2 causes the pre-SN model to become redder. On the other hand, for a fixed value of f_{sh} and primary mass, increasing M_2 (Fig. 9) causes the envelope mass to increase. As the envelope-to-core mass ratio increases, the post-merger stars appear hotter and more luminous throughout their evolution.

We arrive at two results at this point. Firstly, in order to obtain high values of N/C and N/O at the surface and high values of T_{eff} and L required for the progenitor of SN 1987A, we need to restrict the mixing boundary m_b to be inside the He shell or on the He core boundary. Secondly, without He core penetration during the merger, the post-merger stars evolve as cool RSGs until they explode. Thus accretion alone does not suffice to make blue stars. Let us now understand how varying f_{sh} and M_2 for a particular M_1 affects the evolution of the post-merger star.

From Fig. 10, we see that for a fixed combination of M_1 and M_2, increasing f_{sh} makes the pre-SN model cooler. On the other hand, for a fixed value of f_{sh}, increasing M_2 increases the envelope mass and makes the final model hotter and also more luminous.

We now arrive at our next set of conclusions. A merged star is most likely to end its life as a BSG and have high values of N/C and N/O in the surface across all values of M_1 and M_2 used in this study, if f_{sh} is between 10 per cent and 50 per cent. The frequency of cooler stars ($T_{eff} < 12$ kK) increases as M_1 and f_{sh} increase and M_2

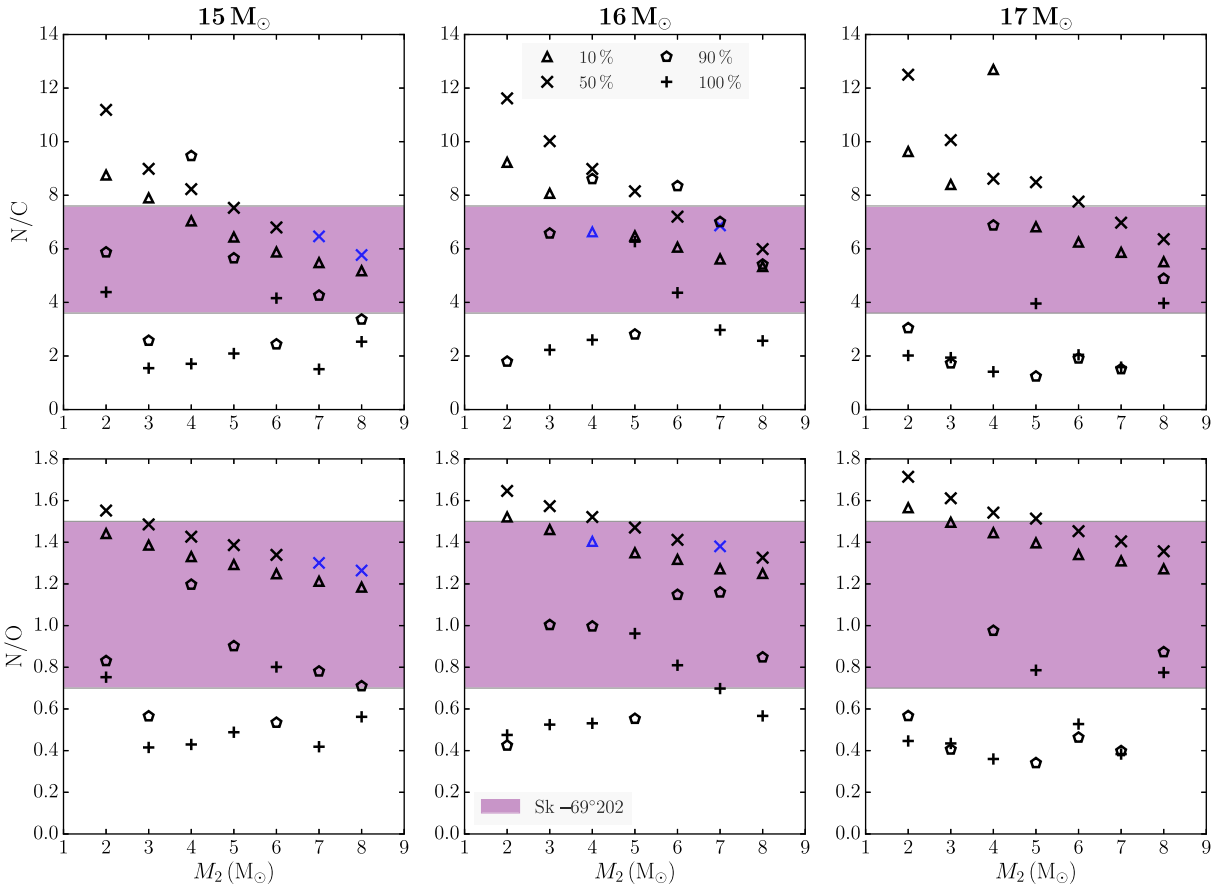

Figure 6. Distribution of number ratios, N/C and N/O of all final models for each of the primary masses, M_1. These parameters are plotted in a column for each M_1 against the range of M_2. The symbols stand for different values of f_{sh}. The bold blue symbols are progenitor models for SN 1987A that satisfy criteria (i)–(iii) in Section 3.1. The shaded violet region denotes the observation limits as explained in Fig. 5.

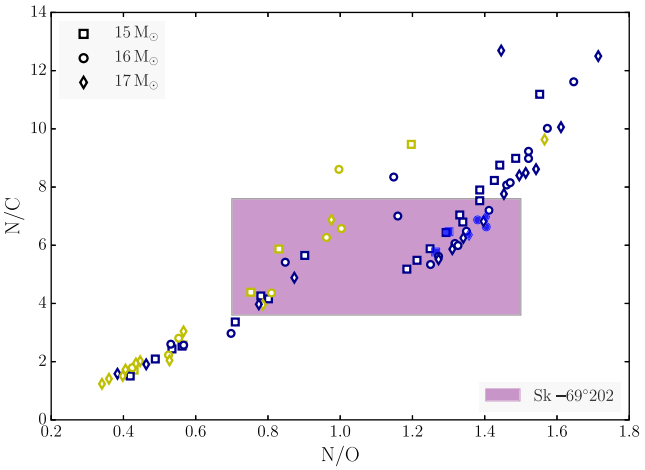

Figure 7. Distribution of number ratios N/C versus N/O at the surface of all 84 models computed. The shaded violet region denotes the observation limits for Sk –69 °202 as in Fig. 5. Yellow symbols are YSGs, blue symbols are BSGs and filled blue symbols are progenitor models for SN 1987A that satisfy conditions (i)–(iii) in Section 3.1.

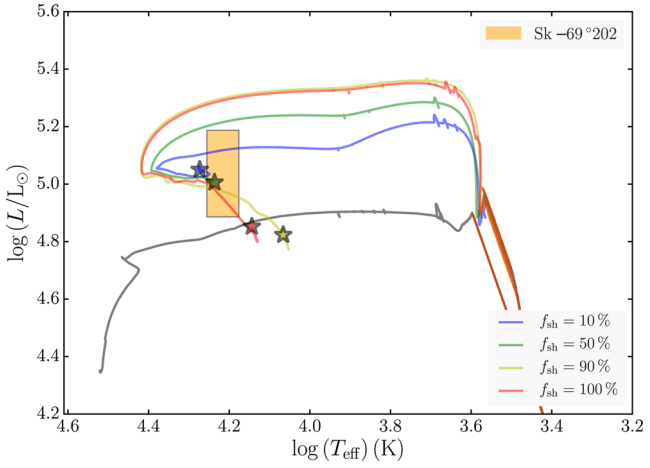

Figure 8. The evolutionary tracks of four cases computed for the merger of $M_1 = 16$ and $M_2 = 6\,M_\odot$, with $f_{sh} = 10$ per cent, 50 per cent, 90 per cent and 100 per cent. Stars denote the final models of individual evolutionary tracks. The shaded orange region denotes the observation limits as in Fig. 5.

decreases. The most crucial initial parameter that affects T_{eff} of the pre-SN model is f_{sh}, which determines the He core mass, followed by M_2, which determines the envelope mass and, finally, M_1. This suggests that there must exist an underlying connection between T_{eff} and envelope-to-core mass ratio of the post-merger star.

3.2.3 *Lifetime of BSG model before explosion*

We address the final quantity measured for Sk –69 °202 – the duration of the BSG phase of the progenitor, τ_{BSG}. We calculate τ_{BSG} as the period when the post-merger star attains $T_{eff} = 12$ kK until

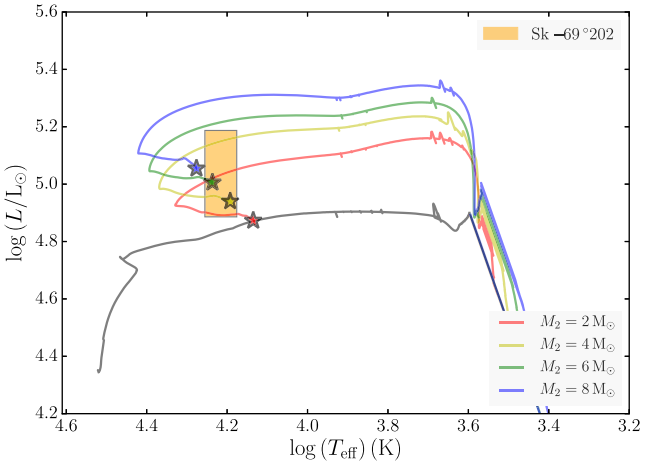

Figure 9. The evolutionary tracks of four cases computed for the merger of $M_1 = 16\,M_\odot$ with $M_2 = 2$, 4, 6 and $8\,M_\odot$, and $f_{\rm sh} = 50$ per cent. Stars denote the final models of individual evolutionary tracks. The shaded orange region denotes the observation limits as in Fig. 5.

the time of its explosion. From Table 4, our BSG progenitors for SN 1987A have lifetimes that are larger than 15–20 kyr expected from observations (and is the case for all the BSG pre-SN models obtained in this study, see Appendix A). This parameter, however, does not depend on the three initial parameters we varied, but, in fact, on the age of the primary RSG model just before the merger begins. The younger the RSG model is (the earlier along the giant branch it is), the longer the post-merger remnant lives as a BSG. The further along the giant branch the primary RSG is, the closer the core gets to carbon ignition. A proxy for the age of the RSG model is the mass fraction of helium at the centre ($X_{\rm He\,c,\,1}$), which decreases as the RSG model grows older. The RSG primary models in this study were chosen when $X_{\rm He\,c,\,1} \sim 10^{-2}$. We compute pre-SN models from a particular initial system of $M_1 = 16\,M_\odot$, $M_2 = 6\,M_\odot$ and $f_{\rm sh} = 50$ per cent, by choosing primary RSG models with decreasing values of $X_{\rm He\,c,1}$. From Table 5, we see that for $X_{\rm He\,c,1} \leqq 10^{-4}$, $\tau_{\rm BSG}$ reduces from 48 kyr, to 17.1 kyr − 18.3 kyr. The other parameters of the pre-SN model are largely unaffected.

We have thus demonstrated that it is possible to obtain BSG progenitors for Type II SNe, with a range of luminosities, effective temperatures, envelope compositions and durations of the BSG phase from various combinations of initial parameters for binary mergers. We summarize our results in Section 4.

4 DISCUSSIONS AND CONCLUSIONS

In this paper, we present Type II SN progenitors from the first detailed stellar evolution study of binary mergers of massive stars. Our pre-SN models span a large range of N/C and N/O ratios at the surface, demonstrating that chemical abundances and the position in the HRD of the progenitor are independent constraints. We can simultaneously reproduce the three key signatures of Sk –69 °202 in our pre-SN models- the position of Sk –69 °202 in the HRD, its surface number ratios and its lifetime before exploding as SN 1987A.

We provide details of the 84 models computed in Appendix A. These merger models were evolved until prior to the collapse of the iron core, from a parameter space consisting of the primary mass $M_1 = 15$–$17\,M_\odot$, the secondary mass $M_2 = 2$–$8\,M_\odot$ and the fraction of He shell dredged up from the He core, $f_{\rm sh} = 10$ per cent, 50 per cent, 90 per cent and 100 per cent. Within the evolutionary scenario and parameter space explored, we find that Sk –69 °202 can be reproduced with different combinations of the above three parameters. The nature of the pre-SN models rely only on the choice of these three parameters and no additional fine-tuning is required during the evolution of the star to produce BSGs. The majority of the final models are BSGs (59 out of 84) while the rest are YSGs. This leads us to conclude that the progenitors of Type II-pec SNe are highly favoured outcomes from a binary merger.

We draw the following inferences from our results:

(i) The parameter of paramount importance, which determines how hot the surface of the pre-SN model is, is $f_{\rm sh}$. Across the range of primary and secondary masses chosen, BSG (with $T_{\rm eff} \geqq 12$ kK) are produced when $f_{\rm sh} \leqq 50$ per cent. Since dredge-up is restricted to the nitrogen-rich region of the He shell, these values of fsh also result in high enough values of N/C and N/O in the surface, required for Sk –69 °202.

(ii) The second parameter of importance is the mass of the secondary star, M_2. Increasing M_2 for a fixed value of $f_{\rm sh}$ (which determines the post-merger He core mass) increases the $T_{\rm eff}$ of the pre-SN star but decreases N/C and N/O in the surface.

(iii) Finally, the parameter that affects the lifetime of the BSG star before its explosion is the age of the primary RSG model at the time of the merger. For a given M_1, older the RSG model is at the time of the merger, shorter the lifetime of the BSG after the merger. Thus for any initial system, the lifetime of the BSG models can be reduced to 15-20 kyr as expected for Sk –69 °202, by choosing older RSG models. This choice of the RSG model, does not significantly affect the surface quantities of the pre-SN model.

(iv) YSG progenitors are produced when either $M_2 = 2\,M_\odot$ or for small He cores, i.e. when $f_{\rm sh} > 50$ per cent. These models increase in number as M_1 increases. The only condition under which RSG progenitors are produced is when the mixing boundary is set above the He core, i.e. the He core is not penetrated in the merger.

(v) The only condition under which RSG pre-SN models are produced is when the mixing boundary is set above the He core, i.e., the He core is not penetrated in the merger. Thus accretion alone does not result in hot, compact progenitors.

(vi) The pre-SN models that match Sk –69 °202 are from the following systems: $M_1 + M_2$ ($f_{\rm sh}$) = $15 + 7\,M_\odot$ (50 per cent), $15 + 8\,M_\odot$ (50 per cent), $16 + 4\,M_\odot$ (10 per cent), $16 + 7\,M_\odot$ (50 per cent), $17 + 7\,M_\odot$ (50 per cent) and $17 + 8\,M_\odot$ (10 per cent).

(vii) BSGs are found to span a large range of N/C and N/O values in the surface (N/C = 1.8–13, N/O = 0.4–1.8), whereas YSGs are found almost entirely within N/C = 1–9.7 and N/O = 0.4–1.0. He/H in the surface is between 0.13–0.17 in all models.

Previous works such as those of Barkat & Wheeler (1989b), Podsiadlowski et al. (1992), Woosley et al. (1997), Vanbeveren et al. (2013) and Petermann et al. (2015), have shown that small He cores and large envelope masses can make stars blue. These works find that reducing the He core to total mass ratio is alone sufficient to make BSGs. Podsiadlowski et al. (1992) found that increasing the accreted secondary mass for a particular He core mass of the primary, increases the $T_{\rm eff}$ of pre-SN models monotonically. They were hence able to determine a critical value for the He core to total mass ratio, below which pre-SN BSGs were possible.

In our study however, we find that with accretion alone, the post-merger stars remain red until the end of their evolution. A necessary condition is the penetration of the He core by the envelope, during the merging process. In fact, for a fixed secondary and primary

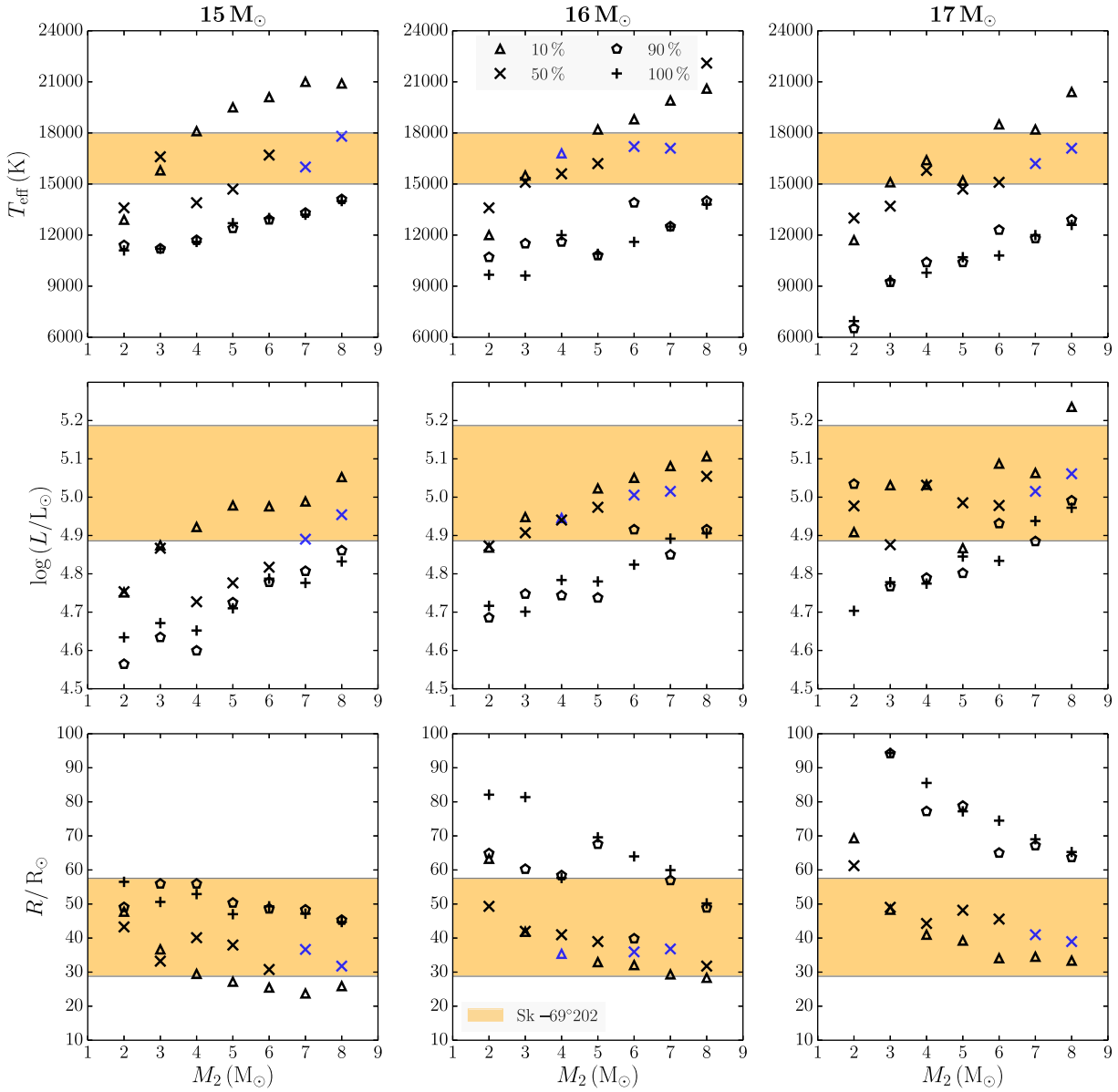

Figure 10. Distribution of effective temperature ($T_{\rm eff}$), luminosity (L) and radius (R) of all models computed. Symbols are as in Fig. 6. The shaded orange region denotes the observation limits as in Fig. 5.

Table 5. Properties of different RSG models of $M_1 = 16\,{\rm M}_\odot$, $\omega/\omega_{\rm crit} = 0.30$ and final models from their merger with $M_2 = 6\,{\rm M}_\odot$ and $f_{\rm sh} = 50$ per cent. $X_{\rm He\,c}$, $\rho_{\rm c}$, $T_{\rm c}$, R and $M_{\rm He\,c,\,1}$ are the central helium mass fraction, central density, central temperature, radius and He core mass of RSG model; log (L), $T_{\rm eff}$, $R_{\rm pre\text{-}SN}$ and $T_{\rm eff}$ are the luminosity, effective temperature and radius of the pre-SN model; N/C, N/O and He/H are the surface number ratios of nitrogen to carbon, nitrogen to oxygen and helium to hydrogen of the pre-SN model; and $\tau_{\rm BSG}$ is the lifetime of BSG before explosion.

$X_{\rm He\,c}$	$\rho_{\rm c}$ (10^3 g cc^{-1})	$T_{\rm c}$ (10^8 K)	$R_{\rm RSG}$ (R⊙)	$M_{\rm He\,c,\,1}$ (M⊙)	log (L) (L⊙)	$T_{\rm eff}$ (kK)	$R_{\rm pre\text{-}SN}$ (R⊙)	N/C	N/O	He/H	$\tau_{\rm BSG}$ (kyr)
10^{-2}	2.5	2.6	607	4.92	4.97	16.7	43.1	8.1	1.5	0.15	48.0
10^{-4}	4.4	3.1	773	4.94	4.94	16.6	36.5	7.6	1.42	0.14	18.3
10^{-6}	5.5	3.3	778	4.94	5.07	16.7	41.4	8.0	1.43	0.14	17.2
10^{-8}	5.5	3.4	824	4.94	5.02	16.3	41.4	8.2	1.43	0.14	17.1

mass, the $T_{\rm eff}$ of the pre-SN model decreases as the mass of the He core decreases with deeper penetration by the envelope. Increasing the secondary mass for a fixed primary mass and penetration depth however, does increase the $T_{\rm eff}$ of the pre-SN models. In our study thus, the final $T_{\rm eff}$ is tied in with two parameters- the fractional decrease of the He core after the merger and the envelope-to-core mass ratio. This is why we do not obtain a monotonic relationship between $T_{\rm eff}$ and the envelope-to-core mass ratio.

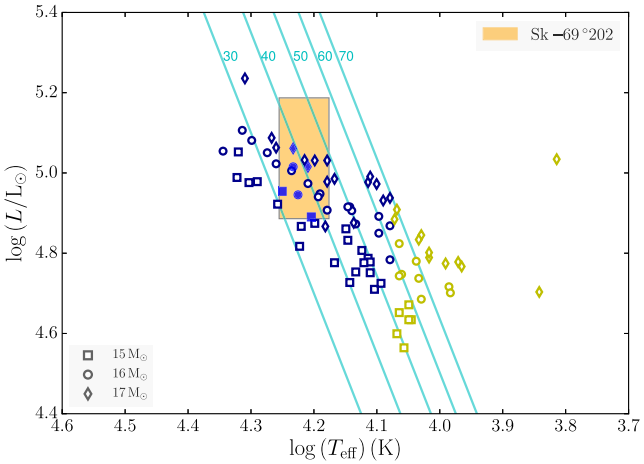

Figure 11. Distribution of all 84 final models in the HRD. Lines of constant surface radius (in $R_\odot$) are drawn. The shaded orange region denotes the observation limits as in Fig. 5. Symbols are as explained in Fig. 7.

There may be other reasons as to why BSGs form. – Ivanova (2002) and Vanbeveren et al. (2013) mention that the sharp rise in the hydrogen profile between the He core and the envelope after the merger or the additional fuel supplied to the H-burning shell may also be causes. We hope that our findings will contribute to the quest of understanding why stars end up becoming becoming BSGs or, for that matter, RSGs.

Using higher mass mergers, we can obtain larger N/O ratios and luminosity, comparable to what is found for Sher 25, which has $\log(L/L_\odot) > 5.78$–5.90 (Smartt et al. 2002; Melena et al. 2008) and N/O $\sim$ 1.7–2.1 (Hendry et al. 2008). In the same vein, we can compare our models with the circumstellar abundances and HRD positions of other BSGs that have ring nebulae around them to confirm their origin from binary mergers.

The majority of Type II-pec SNe found so far have been in low-metallicity galaxies and hence Pastorello et al. (2012) and Taddia et al. (2013) suggest that low metallicities may play a role in forming BSG progenitors. There may be an influence of metallicity on the interactions of binary systems – de Mink, Pols & Yoon (2008) found that case C mass transfers from massive stars are more likely in low-metallicity environments than in those of solar metallicity. Eggenberger, Meynet & Maeder (2002) find that the RSG-to-BSG ratio decreases with metallicity. In our work, the key factor that determines the fate of the pre-SN model is the core-envelope mass ratio of the post-merger star. In order to pursue the question of how likely these mergers are in low-metallicity environments, we need to perform a population synthesis study.

The abundances of Ba and Sr in the surface of our pre-SN models are unchanged from their initial amounts and hence do not exhibit the s-process overabundance detected by Mazzali et al. (1992) and Mazzali & Chugai (1995). More recent studies, such as those by Utrobin & Chugai (2005) and Dessart & Hillier (2008), have shown the importance of time-dependent hydrogen ionization in the evolution of Type II SN spectrum. From the time-dependent ionization models for SN 1987A, Utrobin & Chugai (2005) concluded that the barium abundance in its atmosphere matched the LMC value and was not in fact enhanced.

The N/C and N/O ratios in the surface do not vary much from the end of the merger to core collapse. This may suggest that the outer rings likely formed from material ejected by the wind after the merger, but we cannot provide a more detailed dating based on abundance patterns.

We do not include the spin-up of the CE, or the heating of accreted material in our model, which we intend to look into as part of future work. These effects may affect the evolutionary path of the stars and also help gauge how fast the core will be rotating at the time of explosion.

Mass ejection from the CE phase is not explicitly modelled in this study. Since no circumstellar disc has been found around the remnant, we assume that the material ejected from the CE is in the nebula alone. The effect of mass-loss from the merger is to cause the envelope mass to reduce and thereby decrease the envelope-to-core mass ratio of the post-merger model. We indirectly explore the effect of mass ejection, by accreting a wide range of secondary masses for every primary RSG model, which changes the envelope-to-core mass ratio. Within the range of secondary masses and the age of the primary model at the time of merger, helium is enhanced by a maximum of 9 per cent in the post-merger envelope compared to its initial value. This level of enhancement in helium does not by itself substantially affect the evolutionary path of the post-merger models. We thus rule out the role of helium in obtaining BSGs from mergers.

Overall, our BSG pre-SN models are more massive than single-star progenitor models for SN 1987A. With single-star models, the progenitor mass is determined by first comparing the surface luminosity with the mass of the evolved He core and then determining the initial mass of the progenitor (Woosley et al. 1988; Smartt et al. 2009; Dessart et al. 2010). The reason the He-core mass is strongly correlated to the ZAMS mass of the star is because, in single star models the mass loss from the surface has little effect on the He-core mass (Dessart et al. 2010). The He core mass thus determined for the luminosity of Sk –69 °202 is $M_{\rm He\,c} = 4$–$7\,M_\odot$, which would originate from a ZAMS star of mass, $M_{\rm ZAMS} = 14$–$20\,M_\odot$ (Arnett et al. 1989; Smartt 2009; Smartt et al. 2009). In the case of our merger models, the pre-SN He core mass depends on M_1 and the boundary of mixing, whereas the initial mass is the sum of M_1 and M_2, and, hence, a given He core mass could belong to any number of initial masses depending on the accreted value of M_2.

Consequently, these merger models will impact the parametrized studies of SN explosion properties that are calibrated against supernova SN 1987A such as those of Kleiser et al. (2011). Typical single-star models used for SN 1987A are those from Woosley (1988) and Woosley et al. (1988), $M_{\rm ZAMS} =$ 15–20, $M_{\rm He\,c} = 4.1$–6.2 and $M_{\rm env} = 5$–$10\,M_\odot$ (Arnett et al. 1989; Dessart & Hillier 2010; Utrobin et al. 2015) or the He-enriched models of Nomoto et al. (1988) and Saio et al. (1988), $M_{\rm ZAMS} = 23$, $M_{\rm He\,c} = 6$ and $M_{\rm env} = 10.3\,M_\odot$ (Blinnikov et al. 2000; Kleiser et al. 2011; Ugliano et al. 2012). In contrast to the above single-star models, Utrobin (2004); Utrobin & Chugai (2005) found that a compact, more massive pre-SN model, of $35\,R_\odot$ and $M_{\rm env} = 18\,M_\odot$, fits both the bolometric light curve as well as the H-alpha profile of SN 1987A, with large amounts of mixing of ^{56}Ni.

Our BSG pre-SN models have lower He core masses, $M_{\rm He\,c} = 2.4$–$4.5\,M_\odot$, and much larger envelope masses $M_{\rm env} = 12.3$–$20.5\,M_\odot$. It is therefore imperative to determine the explosion properties of SN 1987A with these models. In a subsequent paper, we will present the light curves and spectra from the explosions of these models using a radiative transfer code and compare them to existing observations of Type II-pec SNe, focusing particularly on SN 1987A.

ACKNOWLEDGEMENTS

The authors would like to thank Luc Dessart for his feedback on the manuscript and understanding conclusions for supernova light curves. We thank Philipp Podsiadlowski for useful discussions about his and Natasha Ivanova's model, on which this paper is based. We also thank Bernhard Müller and John Lattanzio for their feedback and useful comments during the making of this manuscript. We also thank Amanda Karakas, Dorottya Szécsi and Rebecca Nealon for their feedback on previous versions of the manuscript. We thank Thomas Constantino for helping with the opacity tables in KEPLER and Christian Ritter for providing the initial abundance generator tool. This research was supported by US NSF to JINA-CEE through grant PHY-1430152. AH was supported by an ARC Future Fellowship FT120100363.

REFERENCES

Arnett W. D., Bahcall J. N., Kirshner R. P., Woosley S. E., 1989, ARA&A, 27, 629
Asplund M., Grevesse N., Sauval A. J., Scott P., 2009, ARA&A, 47, 481
Barkat Z., Wheeler J. C., 1989a, ApJ, 341, 925
Barkat Z., Wheeler J. C., 1989b, ApJ, 342, 940
Blanco V. M. et al., 1987, ApJ, 320, 589
Blinnikov S., Lundqvist P., Bartunov O., Nomoto K., Iwamoto K., 2000, ApJ, 532, 1132
Brandner W., Grebel E. K., Chu Y.-H., Weis K., 1997a, ApJ, 475, L45
Brandner W., Chu Y.-H., Eisenhauer F., Grebel E. K., Points S. D., 1997b, ApJ, 489, L153
Brott I. et al., 2011, A&A, 530, A116
Burrows C. J. et al., 1995, ApJ, 452, 680
Catchpole R. M. et al., 1988, MNRAS, 231, 75P
Chevalier R. A., Dwarkadas V. V., 1995, ApJ, 452, L45
Chita S. M., Langer N., van Marle A. J., García-Segura G., Heger A., 2008, A&A, 488, L37
Constantino T., Campbell S., Gil-Pons P., Lattanzio J., 2014, ApJ, 784, 56
Crotts A. P. S., Heathcote S. R., 2000, ApJ, 528, 426
Crotts A. P. S., Kunkel W. E., 1991, ApJ, 366, L73
de Mink S. E., Pols O. R., Yoon S.-C., 2008, AIP Conf. Proc. Vol. 990, Binaries at Low Metallicity: Ranges For Case A, B and C Mass Transfer. Am. Inst. Phys., New York, p. 230
Dessart L., Hillier D. J., 2008, MNRAS, 383, 57
Dessart L., Hillier D. J., 2010, MNRAS, 405, 2141
Dessart L., Livne E., Waldman R., 2010, MNRAS, 408, 827
Ferguson J. W., Alexander D. R., Allard F., Barman T., Bodnarik J. G., Hauschildt P. H., Heffner-Wong A., Tamanai A., 2005, ApJ, 623, 585
Eggenberger P., Meynet G., Maeder A., 2002, A&A, 386, 576
Eggleton P. P., Tokovinin A. A., 2008, MNRAS, 389, 869
Folatelli G., Bersten M. C., Kuncarayakti H., Benvenuto O. G., Maeda K., Nomoto K., 2015, ApJ, 811, 147
France K. et al., 2010, Science, 329, 1624
France K. et al., 2011, ApJ, 743, 186
Fransson C., Cassatella A., Gilmozzi R., Kirshner R. P., Panagia N., Sonneborn G., Wamsteker W., 1989, ApJ, 336, 429
Gvaramadze V. V. et al., 2015, MNRAS, 454, 219
Hamuy M., Suntzeff N. B., Gonzalez R., Martin G., 1988, AJ, 95, 63
Heger A., Langer N., 1998, A&A, 334, 210
Heger A., Langer N., 2000, ApJ, 544, 1016
Heger A., Langer N., Woosley S. E., 2000, ApJ, 528, 368
Heger A., Woosley S. E., Rauscher T., Hoffman R. D., Boyes M. M., 2002, New Astron. Rev., 46, 463
Heger A., Woosley S. E., Spruit H. C., 2005, ApJ, 626, 350
Hendry M. A., Smartt S. J., Skillman E. D., Evans C. J., Trundle C., Lennon D. J., Crowther P. A., Hunter I., 2008, MNRAS, 388, 1127
Hillebrandt W., Meyer F., 1989, A&A, 219, L3
Hirschi R., Meynet G., Maeder A., 2004, A&A, 425, 649
Iglesias C. A., Rogers F. J., 1996, ApJ, 464, 943
Ivanova N., 2002, PhD thesis, Univ. Oxford
Ivanova N., Podsiadlowski P., 2002a, in Tout C. A., van Hamme W., eds, ASP Conf. Ser. Vol. 279, Exotic Stars as Challenges to Evolution. Astron. Soc. Pac., San Francisco, p. 245
Ivanova N., Podsiadlowski P., 2002b, Ap&SS, 281, 191
Ivanova N., Podsiadlowski P., 2003, in Hillebrandt W., Leibundgut B., eds, From Twilight to Highlight: The Physics of Supernovae. p. 19
Ivanova N., Podsiadlowski P., Spruit H., 2002, MNRAS, 334, 819
Justham S., Podsiadlowski P., Vink J. S., 2014, ApJ, 796, 121
Kleiser I. K. W. et al., 2011, MNRAS, 415, 372
Kobulnicky H. A., Fryer C. L., 2007, ApJ, 670, 747
Langer N., 1991, A&A, 252, 669
Lundqvist P., Fransson C., 1996, ApJ, 464, 924
McCray R., 1993, ARA&A, 31, 175
Maeder A., 1987, in Danziger I. J., ed., European Southern Observatory Conference and Workshop Proceedings Vol. 26, p. 251
Maran S. P., Sonneborn G., Pun C. S. J., Lundqvist P., Iping R. C., Gull T. R., 2000, ApJ, 545, 390
Marigo P., Aringer B., 2009, A&A, 508, 1539
Mattila S., Lundqvist P., Gröningsson P., Meikle P., Stathakis R., Fransson C., Cannon R., 2010, ApJ, 717, 1140
Mazzali P. A., Chugai N. N., 1995, A&A, 303, 118
Mazzali P. A., Lucy L. B., Butler K., 1992, A&A, 258, 399
Melena N. W., Massey P., Morrell N. I., Zangari A. M., 2008, AJ, 135, 878
Morris T., Podsiadlowski P., 2007, Science, 315, 1103
Morris T., Podsiadlowski P., 2009, MNRAS, 399, 515
Nieuwenhuijzen H., de Jager C., 1990, A&A, 231, 134
Nomoto K., Shigeyama T., Kumaga S., Hashimoto M.-A., 1988, Proc. Astron. Soc. Aust., 7, 490
Panagia N., Scuderi S., Gilmozzi R., Challis P. M., Garnavich P. M., Kirshner R. P., 1996, ApJ, 459, L17
Pastorello A. et al., 2012, A&A, 537, A141
Petermann I., Langer N., Castro N., Fossati L., 2015, A&A, 584, A54
Podsiadlowski P., 1992, PASP, 104, 717
Podsiadlowski P., Joss P. C., 1989, Nature, 338, 401
Podsiadlowski P., Joss P. C., Rappaport S., 1990, A&A, 227, L9
Podsiadlowski P., Joss P. C., Hsu J. J. L., 1992, ApJ, 391, 246
Podsiadlowski P., Morris T. S., Ivanova N., 2006, in Kraus M., Miroshnichenko A. S., eds, ASP Conf. Ser. Vol. 355, Stars with the B[e] Phenomenon. Astron. Soc. Pac., San Francisco, p. 259
Podsiadlowski P., Morris T. S., Ivanova N., 2007, in Immler S., Weiler K., McCray R., eds, Am. Inst. Phys. Conf. Ser. Vol. 937, Supernova 1987A: 20 Years After: Supernovae and Gamma-Ray Bursters. Am. Inst. Phys., New York, p. 125
Popova E. I., Tutukov A. V., Yungelson L. R., 1982, Ap&SS, 88, 55
Potekhin A. Y., Chabrier G., Lai D., Ho W. C. G., van Adelsberg M., 2006, J. Phys. A: Math. Theor., 39, 4453
Rauscher T., Heger A., Hoffman R. D., Woosley S. E., 2002, ApJ, 576, 323
Saio H., Nomoto K., Kato M., 1988, ApJ, 331, 388
Sana H. et al., 2012, Science, 337, 444
Sana H. et al., 2013, A&A, 550, A107
Smartt S. J., 2009, ARA&A, 47, 63
Smartt S. J., Lennon D. J., Kudritzki R. P., Rosales F., Ryans R. S. I., Wright N., 2002, A&A, 391, 979
Smartt S. J., Eldridge J. J., Crockett R. M., Maund J. R., 2009, MNRAS, 395, 1409
Smith N., 2007, AJ, 133, 1034
Smith L. J., Nota A., Pasquali A., Leitherer C., Clampin M., Crowther P. A., 1998, ApJ, 503, 278
Smith N., Arnett W. D., Bally J., Ginsburg A., Filippenko A. V., 2013, MNRAS, 429, 1324
Smith N., Groh J. H., France K., McCray R., 2017, MNRAS, 468, 2333
Sonneborn G., Fransson C., Lundqvist P. A., Cassatella A., Gilmozzi R., Kirshner R. P., Panagia N., Wamsteker W., 1997, ApJ, 477, 848
Sugerman B. E. K., Crotts A. P. S., Kunkel W. E., Heathcote S. R., Lawrence S. S., 2005a, ApJS, 159, 60

Sugerman B. E. K., Crotts A. P. S., Kunkel W. E., Heathcote S. R., Lawrence S. S., 2005b, ApJ, 627, 888
Taddia F. et al., 2013, A&A, 558, A143
Tutukov A. V., Yungelson L. R., Iben I. Jr., 1992, ApJ, 386, 197
Ugliano M., Janka H.-T., Marek A., Arcones A., 2012, ApJ, 757, 69
Utrobin V. P., 2004, Astron. Lett., 30, 293
Utrobin V. P., Chugai N. N., 2005, A&A, 441, 271
Utrobin V. P., Wongwathanarat A., Janka H.-T., Müller E., 2015, A&A, 581, A40
Vanbeveren D., Mennekens N., Van Rensbergen W., De Loore C., 2013, A&A, 552, A105
Walborn N. R., Lasker B. M., Laidler V. G., Chu Y.-H., 1987, ApJ, 321, L41
Walborn N. R., Prevot M. L., Prevot L., Wamsteker W., Gonzalez R., Gilmozzi R., Fitzpatrick E. L., 1989, A&A, 219, 229
Wampler E. J., Wang L., Baade D., Banse K., D'Odorico S., Gouiffes C., Tarenghi M., 1990, ApJ, 362, L13
Weiss A., Hillebrandt W., Truran J. W., 1988, A&A, 197, L11
West R. M., Lauberts A., Schuster H.-E., Jorgensen H. E., 1987, A&A, 177, L1
Wood P. R., 1988, Proc. Astron. Soc. Aust., 7, 386
Woosley S. E., 1988, ApJ, 330, 218
Woosley S. E., Heger A., 2007, Phys. Rep., 442, 269
Woosley S. E., Pinto P. A., Weaver T. A., 1988, Proc. Astron. Soc. Aust., 7, 355
Woosley S. E., Heger A., Weaver T. A., Langer N., 1997, preprint (arXiv:e-prints)
Woosley S. E., Heger A., Weaver T. A., 2002, Rev. Mod. Phys., 74, 1015

APPENDIX A

This section contains the properties of all the pre-SN models computed in this study.

Table A1. Parameters of BSG binary merger progenitors of Type II SNe ($T_{\rm eff} \geq 12$ kK). Column headings are the same as in Table 4.

M_1 ($M_\odot$)	M_2 ($M_\odot$)	$f_{\rm sh}$ (per cent)	$f_{\rm c}$ (per cent)	$m_{\rm b}$ ($M_\odot$)	$M_{\rm He\,c}$ ($M_\odot$)	$M_{\rm env}$ ($M_\odot$)	$M_{\rm pre\text{-}SN}$ ($M_\odot$)	$T_{\rm eff}$ (kK)	$\log(L)$ ($L_\odot$)	$R_{\rm pre\text{-}SN}$ ($R_\odot$)	$M_{\rm Fe\,c}$ ($M_\odot$)	N/C	N/O	He/H	$\tau_{\rm BSG}$ (kyr)
15	2	10	3.5	4.29	3.75	12.33	16.08	12.9	4.75	47.8	1.49	8.8	1.4	0.14	85
15	2	50	17.5	3.67	3.40	12.71	16.09	13.6	4.75	43.3	–	11.2	1.6	0.15	76
15	3	10	3.5	4.29	3.67	13.41	17.08	15.8	4.87	36.7	1.51	7.9	1.4	0.13	65
15	3	50	17.5	3.67	3.40	13.68	17.08	16.6	4.87	33.2	–	9.0	1.5	0.15	78
15	4	10	3.5	4.29	3.65	14.43	18.08	18.1	4.92	29.5	–	7.0	1.3	0.13	66
15	4	50	17.5	3.67	2.85	15.22	18.07	13.9	4.73	40.1	–	8.2	1.4	0.14	101
15	5	10	3.5	4.29	3.51	15.56	19.07	19.5	4.98	27.2	–	6.4	1.3	0.13	71
15	5	50	17.5	3.67	2.86	16.21	19.07	14.7	4.78	38.0	1.42	7.5	1.4	0.14	105
15	5	100	35.0	2.89	2.35	16.70	19.05	12.7	4.71	47.1	–	2.1	0.5	0.15	149
15	5	90	31.5	3.05	2.59	16.47	19.06	12.4	4.72	50.4	–	5.6	0.9	0.15	104
15	6	10	3.5	4.29	3.57	16.50	20.07	20.1	4.98	25.5	–	5.9	1.2	0.12	71
15	6	50	17.5	3.67	3.00	17.07	20.07	16.7	4.82	30.8	1.43	6.8	1.3	0.14	77
15	6	100	35.0	2.89	2.65	17.40	20.05	13.0	4.79	49.4	–	4.2	0.8	0.15	95
15	6	90	31.5	3.05	2.44	17.61	20.05	12.9	4.78	48.6	–	2.4	0.5	0.15	133
15	7	10	3.5	4.29	3.57	17.49	21.06	21.0	4.99	23.7	1.44	5.5	1.2	0.07	82
15	7	50	17.5	3.67	2.90	18.16	21.06	16.0	4.89	36.7	1.50	6.5	1.3	0.13	82
15	7	100	35.0	2.89	2.40	18.63	21.03	13.2	4.78	47.2	–	1.5	0.4	0.15	132
15	7	90	31.5	3.05	2.50	18.55	21.05	13.3	4.81	48.3	–	4.3	0.8	0.14	126
15	8	10	3.5	4.29	3.32	18.73	22.05	20.9	5.05	25.9	–	5.2	1.2	0.12	69
15	8	50	17.5	3.67	2.95	19.10	22.05	17.8	4.95	31.8	1.45	5.8	1.3	0.13	83
15	8	100	35.0	2.89	2.35	19.68	22.03	14.0	4.83	44.7	–	2.5	0.6	0.14	133
15	8	90	31.5	3.05	2.56	19.48	22.04	14.1	4.86	45.3	–	3.4	0.7	0.14	102
16	2	10	3.3	4.71	4.16	12.85	17.01	12.0	4.87	63.3	–	9.2	1.5	0.14	38
16	2	50	16.6	4.06	3.73	13.28	17.01	13.6	4.87	49.4	–	11.6	1.6	0.16	62
16	3	10	3.3	4.71	4.15	13.85	18.00	15.5	4.95	41.9	1.59	8.1	1.5	0.14	66
16	3	50	16.6	4.06	3.60	14.40	18.00	15.1	4.91	42.0	1.44	10.0	1.6	0.15	68
16	4	10	3.3	4.71	4.11	14.89	19.00	16.8	4.95	35.4	1.58	6.6	1.4	0.13	41
16	4	50	16.6	4.06	3.63	15.37	19.00	15.6	4.94	41.0	1.50	9.0	1.5	0.15	48
16	4	100	33.2	3.25	2.86	16.12	18.98	12.0	4.78	57.7	–	2.6	0.5	0.17	106
16	5	10	3.3	4.71	4.05	15.94	19.99	18.2	5.02	32.9	1.51	6.5	1.3	0.13	51
16	5	50	16.6	4.06	3.65	16.34	19.99	16.2	4.97	39.0	1.50	8.1	1.5	0.15	47
16	6	10	3.3	4.71	3.97	17.02	20.99	18.8	5.05	32.1	1.36	6.1	1.3	0.13	55
16	6	50	16.6	4.06	3.61	17.38	20.99	17.2	5.01	36.0	1.46	7.2	1.4	0.14	48
16	6	90	30.0	3.41	3.09	17.89	20.98	13.9	4.92	39.9	1.37	8.3	1.1	0.15	74
16	7	10	3.3	4.71	3.85	18.14	21.99	19.9	5.08	29.4	1.53	5.6	1.3	0.13	41
16	7	50	16.6	4.06	3.41	18.57	21.98	17.1	5.02	36.8	1.03	6.9	1.4	0.14	49
16	7	100	33.2	3.25	2.98	18.99	21.97	12.5	4.89	60.0	–	3.0	0.7	0.15	63
16	7	90	30.0	3.41	2.82	19.15	21.97	12.5	4.85	57.0	1.53	7.0	1.2	0.15	67
16	8	10	3.3	4.71	3.84	19.14	22.98	20.6	5.11	28.3	–	5.3	1.2	0.13	42
16	8	50	16.6	4.06	3.52	19.45	22.97	22.1	5.05	31.8	–	6.0	1.3	0.13	60
16	8	100	33.2	3.25	2.91	20.04	22.95	13.8	4.91	50.2	–	2.6	0.6	0.15	87
16	8	90	30.0	3.41	2.93	20.03	22.96	14.0	4.92	48.9	1.49	5.4	0.8	0.15	89
17	2	50	15.6	4.44	4.07	13.77	17.84	13.0	4.98	61.3	1.62	12.5	1.7	0.17	40
17	3	10	3.1	5.10	4.62	14.22	18.84	15.1	5.03	48.3	–	8.4	1.5	0.14	34
17	3	50	15.6	4.44	4.24	14.59	18.84	13.7	4.88	49.1	1.53	10.1	1.6	0.16	39
17	4	10	3.1	5.10	4.49	15.35	19.84	16.4	5.03	41.0	–	12.7	1.4	0.14	36
17	4	50	15.6	4.44	4.30	15.53	19.83	15.8	5.03	44.3	1.55	8.6	1.5	0.15	37
17	5	10	3.1	5.10	4.48	16.35	20.83	15.2	4.87	39.3	1.55	6.8	1.4	0.14	39
17	5	50	15.6	4.44	3.93	16.90	20.83	14.7	4.99	48.2	1.52	8.5	1.5	0.15	41
17	6	10	3.1	5.10	4.34	17.48	21.82	18.5	5.09	34.1	–	6.2	1.3	0.13	35
17	6	50	15.6	4.44	3.88	17.94	21.82	15.1	4.98	45.6	1.52	7.8	1.5	0.14	41
17	6	90	28.1	3.78	3.29	18.51	21.80	12.3	4.93	65.0	–	1.9	0.5	0.16	57
17	7	10	3.1	5.10	4.25	18.57	22.82	18.2	5.06	34.5	1.62	5.9	1.3	0.13	39
17	7	50	15.6	4.44	3.86	18.95	22.81	16.2	5.02	41.0	1.53	7.0	1.4	0.14	41
17	7	100	31.2	3.62	3.21	19.60	22.79	12.0	4.94	69.1	1.48	1.6	0.4	0.16	54
17	8	10	3.1	5.10	4.24	19.57	23.81	20.4	5.24	33.4	–	5.5	1.3	0.13	40
17	8	50	15.6	4.44	3.83	19.98	23.81	17.1	5.06	39.0	1.67	6.4	1.4	0.14	41
17	8	100	31.2	3.62	3.32	20.47	23.79	12.6	4.97	65.3	1.48	4.0	0.8	0.15	50
17	8	90	28.1	3.78	3.35	20.44	23.79	12.9	4.99	63.7	1.49	4.9	0.9	0.15	54

Table A2. Parameters of YSG binary merger progenitors of Type II SNe ($4 \leq T_{\rm eff} < 12$ kK). Column headings are the same as Table A1.

M_1 ($M_\odot$)	M_2 ($M_\odot$)	$f_{\rm sh}$ (per cent)	$f_{\rm c}$ (per cent)	$m_{\rm b}$ ($M_\odot$)	$M_{\rm He\,c}$ ($M_\odot$)	$M_{\rm env}$ ($M_\odot$)	$M_{\rm pre\text{-}SN}$ ($M_\odot$)	$T_{\rm eff}$ (kK)	log (L) ($L_\odot$)	$R_{\rm pre\text{-}SN}$ ($R_\odot$)	$M_{\rm Fe\,c}$ ($M_\odot$)	N/C	N/O	He/H	$\tau_{\rm BSG}$ (kyr)
15	2	100	35.0	2.89	2.68	13.40	16.08	11.1	4.63	56.5	1.41	4.4	0.8	0.17	0.0
15	2	90	31.5	3.05	2.67	14.13	16.80	11.4	4.56	49.1	–	5.9	0.8	0.17	0.0
15	3	100	35.0	2.89	2.51	14.55	17.06	11.2	4.67	50.6	–	1.5	0.4	0.17	0.0
15	3	90	31.5	3.05	2.67	14.40	17.07	11.2	4.63	56.0	–	2.6	0.6	0.17	0.0
15	4	100	35.0	2.89	2.46	15.60	18.06	11.6	4.65	52.9	1.41	1.7	0.4	0.16	0.0
15	4	90	31.5	3.05	2.74	15.33	18.07	11.7	4.60	56.0	–	9.5	1.2	0.16	0.0
16	2	100	33.2	3.25	3.14	13.86	17.00	9.67	4.72	82.2	–	20.4	0.5	0.18	0.0
16	2	90	30.0	3.41	3.05	13.95	17.00	10.7	4.69	64.9	–	1.8	0.4	0.18	0.0
16	3	100	33.2	3.25	3.05	14.94	17.99	9.62	4.70	81.4	–	2.2	0.5	0.17	0.0
16	3	90	30.0	3.41	3.10	14.90	18.00	11.5	4.75	60.3	–	6.6	1.0	0.17	0.0
16	4	90	30.0	3.41	3.04	15.96	19.00	11.6	4.74	58.4	–	8.6	1.0	0.16	0.0
16	5	100	33.2	3.25	3.06	16.93	19.99	10.9	4.78	69.6	–	6.3	1.0	0.16	0.0
16	5	90	30.0	3.41	3.00	16.98	19.98	10.8	4.74	67.6	1.34	2.8	0.6	0.16	0.0
16	6	100	33.2	3.25	3.06	17.92	20.98	11.6	4.82	64.0	1.38	4.4	0.8	0.16	0.0
17	2	10	3.1	5.10	4.63	13.21	17.84	11.7	4.91	69.4	1.67	9.6	1.6	0.15	0.0
17	2	90	28.1	3.78	3.46	14.37	17.83	6.52	5.03	177.0	1.51	3.0	0.6	0.19	0.0
17	2	100	31.2	3.62	3.44	14.39	17.83	6.95	4.70	156.8	1.48	2.0	0.4	0.19	0.0
17	3	100	31.2	3.62	3.39	15.43	18.82	9.35	4.78	94.4	1.49	1.9	0.4	0.18	0.0
17	3	90	28.1	3.78	3.37	15.45	18.82	9.23	4.77	94.2	1.44	1.7	0.4	0.18	0.0
17	4	100	31.2	3.62	3.30	16.51	19.81	9.79	4.77	85.6	1.47	1.4	0.4	0.17	0.0
17	4	90	28.1	3.78	3.41	16.41	19.82	10.4	4.79	77.3	1.49	6.9	1.0	0.17	0.0
17	5	100	31.2	3.62	3.39	17.42	20.81	10.7	4.85	77.3	1.50	4.0	0.8	0.17	0.0
17	5	90	28.1	3.78	3.17	17.64	20.81	10.4	4.80	78.8	1.45	1.2	0.3	0.17	0.0
17	6	100	31.2	3.62	3.35	18.45	21.80	10.8	4.83	74.5	1.49	2.0	0.5	0.16	0.0
17	7	90	28.1	3.78	3.22	19.57	22.79	11.8	4.88	67.2	1.47	1.5	0.4	0.16	0.0

This paper has been typeset from a TEX/LATEX file prepared by the author.